Addis Ababa University
Addis Ababa Institute of Technology
School of Multidisciplinary Engineering
Center for Renewable Energy

Numerical Simulation and Performance Investigation of Bubble Pump Refrigerator

A thesis submitted to the Post Graduate Program Office of Addis Ababa Institute of Technology, Addis Ababa University in partial fulfillment of the requirements for the award of Masters of Science in Energy Technologies.

By:
Henok Habte (GSR/7443/12)

Advisor: Solomon T/mariam (PhD)

October, 2023

CERTIFICATION

I, the undersigned, certify that I read and hear by recommend for the acceptance by Addis Ababa University, Addis Ababa Institute of Technology, Center of Renewable Energy a thesis entitled, "Parametric Study of Solar Driven Bubble Pump Refrigerator". This certificate used as a partial fulfillment of the requirement for the degree of Master of Science in Energy Technologies.

Signature _____

Date _____

DECLARATION

I, Henok Habte, declare that this thesis is the result of my own work and that all source and material used for this thesis have been duly acknowledged. This thesis is submitted in partial fulfillment of the requirement for master's degree in renewable energy technology at Addis Ababa University and to be made available at the university's library under the role of the library. I confidently declare that this thesis has not been submitted to any institutions anywhere for the award of any academic degree, diploma, or certificate.

Candidate

Name: Henok Habte

Signature _____

Date _____

Advisor

Name: Solomon T/mariam (PhD)

Signature _____

Date _____

Addis Ababa University

Addis Ababa Institute of Technology

School of Multidisciplinary Engineering

Center for Renewable Energy

Numerical Simulation and Performance Investigation of Bubble Pump Refrigerator

By: Henok Habte

Approved by Board of Examiners

Advisor	Signature	Date
Misrak Girma (PhD)		10/24/2023
External Examiner	Signature	Date
Internal Examiner	Signature	Date
Chairman	Signature	Date
Director of Post Graduate Program	Signature	Date

ACKNOWLEDGEMENT

I want to start by thanking my Lord and Savior for supporting me in this effort from beginning to end. His unending mercy and forgiveness are always a source of strength for me. Second, I want to express my sincere gratitude to Dr. Solomon T/mariam, my advisor and head of the renewable energy center, who made this research possible. His helpful feedback, direction, and mentorship have been crucial to the success of this work. I also want to express my gratitude for his patience in helping me complete this task. Last but not least, I want to express my sincere appreciation to my parents, siblings, and friends who had encouraged me to finish this work and provided me with their kind support.

ABSTRACT

Approximately 30% of the primary energy consumed worldwide is used for refrigeration. In light of the global search for sustainable energy sources and energy-efficient methods of operation, solar-powered bubble pump refrigeration systems have gained traction as an alternative means of satisfying cooling requirements. Diffusion absorption refrigerators, sometimes referred to as bubble pump refrigerators, are driven by low-grade energy sources such as solar, waste heat, and recovery heat and do not require any mechanical moving components. However, in comparison to other cooling options, this system's coefficient of performance (COP) has been low. To increase the system's efficiency, more research on the effects of various parameters is required. The objective of this study is to enhance understanding of the behavior of the system through an examination of the impact of several critical factors. Using the programs ASPEN PLUS and EES, a thorough numerical simulation was conducted after a thermodynamic and system model was created. Every simulation was run with a standard total pressure of 25 bars. The model was used to forecast how different factors, such as generator heat, concentration of the refrigerant in a rich solution, and refrigerant purity, would affect the system's performance. The significant impact of refrigerant purity at the rectifier's outlet on coefficient of performance (COP) was one of the key finding. It was discovered that the COP rose from 0.15 to 0.36 as the purity improved from 0.950 to 0.999. It was also noted that a generator temperature of 200^{o}C at 240W of thermal input was optimal at 25 bars of total system pressure. Additional heat rises did not appear to have a noticeable impact on the performance of the system. The one thing that makes this research stand out is the study of the effect of hydrogen on the COP of the system. It was observed that both heat absorbed at the evaporator (Q_{evap}) and COP increased steadily and with similar degree of increments as hydrogen mass fraction increased from 0.5 to 0.95. This is due to the higher reduction of the partial of the refrigerant at evaporator inlet causing the refrigerant to lower its temperature further. Generally speaking, with more research done, the bubble pump refrigeration holds a lot of potential to take the place of traditional cooling technologies.

Key Words: Bubble pump, Planten-Munter principle, Solar refrigeration, Simulation

TABLE OF CONTENTS

CERTIFICATION I
DECLARATION II
ACKNOWLEDGEMENT IV
ABSTRACT V
TABLE OF CONTENTS VI
NOMENCLATURE VIII
LIST OF FIGURES XI
LIST OF TABLES XIII
1 INTRODUCTION 1
1.1 Background 1
1.2 Problem Statement 3
1.3 Objectives 3
1.4 Delimitation 4
1.5 Organization of the Research 4
2 LITERATURE REVIEW 5
2.1 Solar Cooling Technologies 5
2.2 The Planten-Munter Principle of Bubble Pump Absorption 5
2.3 Solar Collection Technologies 6
2.3.1 Photovoltaic cell 6
2.3.2 Solar thermal 7
2.4 Working Fluids Thermodynamic Property Model 10
2.5 Diffusion Absorption Refrigeration Cycle 15
3 METHOD AND METHODOLOGY 33
3.1 The Choice of Simulation Tool 34
3.2 Selection of Working Fluids 34
3.2.1 Refrigerant 34
3.2.2 Absorbents 35
3.2.3 Refrigerant- Absorbents mixture 35
3.3 Selection of Thermodynamic Property 38
3.4 System Configuration 38
3.5 Thermal Modeling and Governing Equations 40
3.5.1 Generator and Bubble Pump as Unit 41
3.5.2 Rectifier 41

3.5.3 Condenser 41
3.5.4 Evaporator and Gas Heat Exchanger 42
3.5.5 Absorber and Reservoir 42
3.5.6 Solution Heat Exchanger 43
3.6 Components Modeling and Input Data 44
3.6.1 Solution heat exchanger 48
3.6.2 Gas heat exchanger 48
3.6.3 Generator 48
3.6.4 Bubble pump 49
3.6.5 Rectifier 49
3.6.6 Absorber 50
3.6.7 Solution Tank 50
3.6.8 Condenser 51
3.6.9 Evaporator 51
3.7 Hourly Solar Insolation Input 52
3.8 Performance Parameter (COP) 52
3.9 Simulation Procedure 52
4 RESULT AND DISCUSSION 54
4.1 Validation 54
4.2 Results 61
5 CONCLUSION AND RECOMMENDATION 67
REFERENCES 68
APPENDIX A1: ASPEN PLUS SIMULATION RESULT 73
APPENDIX A2: ASPEN PLUS SIMULATION RESULT 77
APPENDIX B: EES code for parametric study 81
APPENDIX C: MeteoNorm weather data for Addis Ababa 86

NOMENCLATURE

Abbreviations

ABS	Absorber
BP	Bubble pump
BPPR	Bubble pump preheater
BZL	Benzoyl
CND	Condenser
COP	Coefficient of performance
DAR	Diffusion absorption refrigeration
DMAC	Dimethylacetamide
DME	Dimethyl ether
DMETEG	Dimethyl ether tetraethylene glycol
DMEU	Dimethylol ethylene urea
DMF	Dimethylformamide
EES	Engineering equation solver
ETC	Evacuated-tube collector
EVAP	Evaporator
FNP	Fraction of non-purchase power
FPC	Flat-Plate collector
FPCI	Flat-Plate collector improved
GEN	Generator
GHX	Gas heat exchanger
HFC	Hydrofloro carbon
I_g	inert gas

L	Liquid
MCL	Methylene chloride
MIXG	Mixer before gas heat exchanger
MXE	Mixer before evaporator
NMP	N-Methyl-2-pyrrolidone
OPEC	Organization of petroleum exporting countries
PT	State Point
QUN	Quinestrol
R12	Dichlorodifluoromethane
SHX	Solution heat exchanger
SOLTANK	Solution tank
TEG	Triethylene glycol
TEGDME	Tetraethylene glycol dimethyl ether
V	Vapor

Symbols

C_p	Specific heat (kj/kg ^oC)
h	Enthalpy (kj/kg)
m	Mass flow rate (kg/hr)
P	Pressure (bar)
Q	Heat (W)
q	vapor fraction
T	Temperature (^oC)

x	ammonia mass fraction in liquid phase
y	ammonia mass fraction in vapor phase

Subscript

abs	Absorber
cond	Condenser
gen	Generator
rect	Rectifier

LIST OF FIGURES

Figure 2-1: Schematic diagram of diffusion absorption machine.....6
Figure 2-2: Schematic diagram of parabolic trough collector 10
Figure 2-3 (a, b, c): T-x-y VLE diagram at P = 2 bar, 10 bar and 25 bar respectively for ammonia-water mixture 14
Figure 3-1: Methodology flowchart.....33
Figure 3-2: Shows the key processes in a typical DAR system using ammonia-water and hydrogen as the auxiliary gas.....39
Figure 3-3: Aspen Plus DAR model 46
Figure 3-4: Solution heat exchanger model in Aspen Plus.....48
Figure 3-5: Gas heat exchanger Aspen Plus model 48
Figure 3-6: Generator Aspen Plus model.....49
Figure 3-7: Bubble pump Aspen Plus model.....49
Figure 3-8: Rectifier model in Aspen Plus 50
Figure 3-9: Absorber model on Aspen Plus.....50
Figure 3-10: Solution tank model in Aspen Plus 51
Figure 3-11: Condenser model in Aspen Plus 51
Figure 3-12: Evaporator model in Aspen Plus.....52
Figure 4-1: Graphical representation of simulated and reference temperatures at state points of the DAR machine.....59
Figure 4-2: Evolution of the partial pressure, vapor fraction, and temperature of the NH_3/H_20 mixture in the evaporator.....60
Figure 4-3: Effect of the generator heat on the generator temperature.....61
Figure 4-4: Effect of refrigerant purity on Qrec, Qevap and Qabs (at Qgen = 100W) 62
Figure 4-5: Effect of refrigerant purity on Qevap and COP 62
Figure 4-6: Effect of refrigerant purity on rectifier exit temperature and the respective COP.....63
Figure 4-7: P-T-x diagram of NH3-H20 solution at 25 bars. 64
Figure 4-8: Effect of mass flow rate of strong solution on Qevap, Qabs, Qcond and Qrec (at Qgen = 100W/kg) 65
Figure 4-9: Effect of hydrogen mass fraction from the absorber outlet on Qevap and COP (Qgen = 50W) 65

Figure 4-10: Effect of mass fraction of ammonia in rich solution on heat rejected, heat absorbed and COP (at Qgen = 50W) 66

LIST OF TABLES

Table 2-1: Solar collector types 8
Table 2-2: Aspen-Plus thermodynamic property models 12
Table 2-3: Literatures reviewed in the area of absorption refrigeration 15
Table 3-1: Summary of some working pairs for absorption systems 35
Table 3-2: Advantages and disadvantages of the two most common working fluid pairs.....37
Table 3-3: State point assumptions for the DAR simulation. 40
Table 3-4: Summery of Aspen-Plus blocks used for the DAR components.....44
Table 3-5: Initial input parameters used in the models of the DAR components.....47
Table 4-1: Aspen-Plus simulation result of the DAR machine.....56
Table 4-2: Aspen Plus simulated results of heat streams.....57
Table 4-3: Comparison of simulated and reference temperatures at different state points.....58
Table 4-4: Comparison of simulated and reference heat stream values 58

1 INTRODUCTION

1.1 Background

As the concern of the world on global climate changes and depleting energy resources increases, solar cooling technologies receive a great interest as an environment-friendly and sustainable alternative. The coincidence of solar intensity and cooling demand has long been inspiring people to invent a machine that cools when the sun shines. Therefore, solar cooling is counter intuitive; cooling something with a heat source. It motivated the first solar cooling machine of the history dating back to 1878 when the French mathematician Augustin Mouchot demonstrated his solar engine with the absorption cooling machine of Edmond Carré to produce ice at the World Exhibition in Paris (Rodríguez-Muñoz & Belman-Flores, 2014). But as energy prices went down with diversifying energy sources and developing transportation technologies, the idea of using solar energy became less attractive. It was in the 1970s that solar cooling received great interest again, when the world suffered from the oil crisis that had been initiated by Arab members of OPEC for political motivations. The world realized that they could no longer depend on cheap oil prices and began to look for alternatives (Tozer & James, 1998).

Solar cooling and refrigeration are used in cooling of buildings of all types, for food preservation, and for storage of vaccines for medical purposes, which is a vital need and an attractive option in many of the developing countries particularly in remote regions with no access to electricity supply (Baldwin & Cruickshank, 2012).

The diffusion (bubble pump) absorption refrigeration (DAR) cycle is a technology of interest for cooling in rural areas and developing countries due to its low capital cost, low maintenance requirements, silent operation and unique design in which the requirement for electrically or mechanically driven components are fully omitted. The diffusion absorption refrigeration (DAR) systems were invented by Von Platen and Munters in the 1920s (Adjibade et al., 2017; Dardouch et al., 2019; Ojha et al., 2020). Its greatest advantage is that it can be run by any source of energy such as electricity, solar power, LPG, natural gas, and waste heat. Two working fluids are used in the DAR system: ammonia as a refrigerant and water as an absorber. Additionally, an inert gas like hydrogen or helium is used as auxiliary gas in this system in order to decrease the partial pressure in the evaporator according to Dalton’s law. Therefore, there are no

moving parts in these systems, and the solution cycle is achieved by heating in the bubble pump (Ben Jemaa et al., 2016; Jelinek et al., 2016; Najjaran et al., 2018; Rodríguez-Muñoz & Belman-Flores, 2014).

Number of numerical and experimental studies has been done on bubble pump absorption refrigeration systems. The common goals of present day research activities on solar assisted DAR are to find, for each different application of cooling, an optimum combination of collector and cooling system that matches the special cooling demands and also the constraints of the available solar radiation in the best way possible (Alazazmeh & Mokheimer, 2015; Benhmidene et al., 2011; Engineering et al., 1999; Shihab & Faisal, 2015; Zulu, 2000).

The disadvantage of DAR, which is used in domestic spaces, is the relatively low coefficient of performance (COP) (Freeman et al., 2017). Other two main reasons that solar DAR are not in widespread use today is the high initial cost and large equipment size. Much of the high cost and bulky equipment is due to the fact that most of the DAR refrigerators built to date have been custom made for the purpose of testing and pilot projects rather than compactness. With additional research, a more compact and inexpensive refrigerators and air conditioner will be produced in the future. A major obstacle in achieving reliable cost effective solar thermal absorption coolers is the problem of adapting individual components of the system to work at the normal working temperatures for solar collectors, between 82 to 121^{o}C. Another challenge is, the solar energy resource available is different at different geographical and climatic locations. Therefore, a parametric analysis of a DAR system specific to Ethiopian different climatic conditions will give a thorough understanding of the system and its feasibility for the Ethiopian market (Ting & Aman, 2016).

Solar cooling technologies have the potential to improve crop and vaccine supply chain management in areas with no or unreliable access to electricity distribution network, a deep understanding of the performance of the system will benefit in future policy making and energy plans for the country.

This research will design a thermal model of a solar-DAR system, which is then used to make a parametric study of the system in steady state using Aspen Plus simulation and EES softwares in order to study the effect of different parameters on the DAR system.

1.2 Problem Statement

As an eco-friendly and sustainable option, solar cooling technology is gaining popularity nowadays. Directly utilizing solar energy as a primary energy source is appealing due to its wide availability, minimal environmental impact, and low or no ongoing fuel expense. This makes it a desirable choice in many developing countries, especially in remote areas without access to an electricity supply. Due to the rising running costs of conventional units, solar thermally powered cooling machines are becoming more and more important now that the price of oil, coal, and natural gas has increased. Technologies that use solar energy combine the benefits of cheap operating costs, widespread energy accessibility, and limitless energy supply. Currently, the solar absorption system stands out as one of the most promising. There are currently much stronger economic and environmental drives to promote solar cooling technology in the market. But both the academic and industrial groups still face difficulties in creating a marketable solar cooling device that is competitive. The low coefficient of performance of the systems, which is in average below 0.15, is one of the challenges to developing reliable and affordable solar absorption refrigerators. To better understand how various parameters affect the system's performance and increase COP, a thorough parametric examination of a bubble pump absorption cooling system powered by solar thermal energy will be conducted in this study. Since the tertiary fluid is a crucial element in such systems, the primary focus of this study will be to understand the effect of Hydrogen, the tertiary fluid in this case, on the COP of the system. This will make it easier to understand the relationships between various parameters and improve optimization for system designs and manufacturing in the future.

1.3 Objectives

The main objective of this research is to numerically simulate and investigate a single total pressure bubble pumped diffusion absorption refrigeration system using solar thermal energy.

Specific Objectives:

The specific objectives of this research are:

- To design and develop a numerical model to analyze the performance of a solar powered bubble pump absorption refrigeration system.
- To choose the right solar collector for the application.

- To choose the most reliable thermodynamic property for the application.
- To study and visualize the expansion process at the inlet of the evaporator that reduces the partial pressure of the refrigerant.
- To study the effect of parameters like hydrogen concentration, refrigerant purity, generator temperature and mass fraction of ammonia on the performance of bubble pump refrigeration system and optimize COP.
- To validate results with other similar research papers.

1.4 Delimitation

This research project is intended to study the influence of hydrogen and different key parameters on the performance of a bubble pump solar absorption machine and find the best configuration for optimum and efficient operation of the system. Recently, different potential working fluids has been studied that could give a better COP for solar DAR systems. However, because of the lack of sufficient data and information on the recently studied working fluids (refrigerant-absorbent-inert gas), this study is limited to the use of only one set of working fluids, i.e. NH_3-H_2O-H_2 and does not cover other types of working fluids. Nonetheless, recent trends of researches involving different working fluids are presented in the literature review section.

1.5 Organization of the Research

The structure of the research is organized as follows: chapter one deals with the introduction of the research which includes background, problem statement, objectives, scope and delimitation of the research. Chapter two discusses previously carried out researches, articles and literatures related to this research paper. The chapter also identified the research gap clearly. Chapter three presents the methods and methodology used in this research paper to carry out the objectives stated in chapter one. It describes how each component is modeled in relation to the Aspen-Plus software and the thermodynamic property used to model the ammonia water binary solution that is used in the simulation environment. It also includes the assumptions used and the initial operating conditions that are applied into the simulation. The fourth chapter deals with results and discussion. Here the results of the simulation and the parametric studies are presented in graphical representation. Validation of the simulation is also presented in this chapter. The last chapter discusses conclusion of the research paper, and recommendations for possible future works.

2 LITERATURE REVIEW

2.1 Solar Cooling Technologies

Solar cooling and refrigeration systems are used to cool space, to preserve food, and to store vaccines and other purposes. It is a vital need and an attractive option in many of the developing countries particularly in remote regions with no access to electricity. Solar cooling technologies have the potential to improve crop and vaccine supply chain management in areas with unreliable access to electricity. The diffusion absorption refrigeration (DAR) cycle is a technology of interest for cooling in rural areas and developing countries due to its low maintenance requirements, and unique design in which the requirement for electrically-driven components are fully omitted (Noor et al., 2016).

2.2 The Planten-Munter Principle of Bubble Pump Absorption

The diffusion absorption refrigeration (DAR) systems were invented by Swedish students called Von Platen and Munters in the 1920s. The disadvantage of DAR is the quite low coefficient of performance (COP) it has; currently ranging from 0.12 to 0.26. Its greatest advantage is that it can be run by different sources of energy such as electricity, solar power, LPG, natural gas, and waste heat. Mainly two working fluids are used in the DAR system: a refrigerant and an absorber. Additionally, inert gas like hydrogen or helium is used as auxiliary gas in the system in order to decrease the partial pressure of the refrigerant in the evaporator according to Dalton's law. Therefore, there are no moving parts in these systems, such as pump or compressor to vary refrigerator pressure in the system. The solution cycle is achieved by heating in the bubble pump and natural flow due to gravity (Alazazmeh & Mokheimer, 2015; Dutil & Rousse, 2010).

Figure 2.1 shows the general configuration of the Platen-Munters DAR system. Main components of the system include a condenser, an evaporator, an absorber, a solution heat exchanger, a rectifier, a reservoir for accumulation of the rich solution and a generator attached to a bubble pump. The bubble pump is the motor of circulation. It's a fluid pump that operates on thermal energy to pump liquid from lower level to the higher level. Its principle of operation differs from that of the conventional absorption refrigeration system that operates based on a dual-pressure cycle and a binary fluid mixture. While DAR is designed for a total single-pressure operation enabled by a third

component (an inert gas), which imposes different partial pressures on the refrigerant. The basic design has not changed much since its invention, which uses ammonia-water-hydrogen as the working fluid at system pressures of 20-25 bar to utilize thermal energy typically at temperatures of 180-250˚C (Freeman et al., 2017). The detail description of the system configuration presented in Figure 2-1 is discussed in section 3.3.

2.3 Solar Collection Technologies

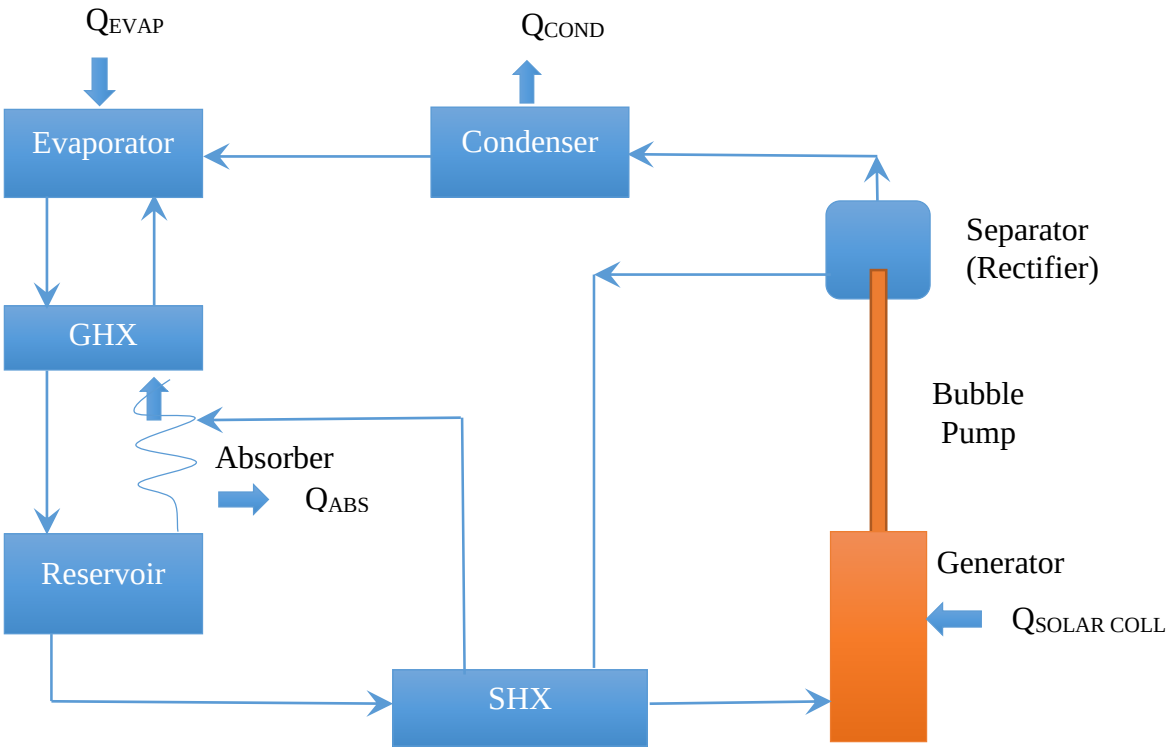

Figure 2-1: Schematic diagram of diffusion absorption machine

Utilization of solar energy requires solar collectors. There are two general types:

I. Photovoltaic cells which can be used to produce electricity.

II. Solar thermal collector which can be utilized to generate heat.

2.3.1 Photovoltaic cell

Photovoltaic cell is a device that converts solar radiation energy directly into electrical energy. The solar cell consists of a disc or surface with two thin layer of differently doped semiconductor material, often silicon, forming a junction in between. Metal stripes runs along the front of the surface and along the back is a metal plate. When solar radiation hits the top of the upper layer, the disc is polarized. The upper layer becomes negatively charged and the lower layer becomes positively charged. If the

metal stripes and plate are connected in a closed circuit, an electrical current will flow through the circuit. Thus, electrical power is accessible. The voltage obtained from a single disc is rather low, in the range of 0.5V. To obtain higher voltage, several discs are connected in series. To increase the current rows of serially connected solar cells can be connected in parallel. Thus, solar cell panels, also called modules, are constructed. The cells are encapsulated in a transparent material (often plastic and low-iron glass) to protect them from the environment (but not to heat insulate them). Several solar cell panels can be combined into a solar cell *array*. This is illustrated in. Commonly the output voltage from solar cell panels seems to be in the range of 12-24 V. In this study solar cells will be referred to only as a source of electric current, hence readers are referred to text books dealing with fundamentals of photovoltaic technology.

2.3.2 Solar thermal

The basic principle of solar thermal collection is that when solar radiation strikes a surface, part of it is absorbed, thereby increasing the temperature of the surface. The central component in each solar collector is the absorber. Here, the absorbed solar radiation is transformed into heat; part of this heat is transferred to the heat transfer fluid and another part is lost to the environment.

2.3.2.1 Classification of solar thermal collectors

Based on the techniques employed in heat collection and losses reduction solar thermal collectors may be classified according (a) their collecting characteristics, (b) operating temperature ranges (c) the way in which they are mounted, and (d) the type of transfer fluid they employ.

A. Collecting characteristics:

i. **A non –concentrating collector** is one in which the absorbing surface for solar radiation is essentially flat with no means for concentrating the incoming solar radiation. These considered are:

- Flat plate collectors: consist of an absorbing surface with passages for heat transfer fluid enclosed in an insulated casing with a transparent cover.
- Evacuated tubular collectors: consist of an absorbing surface mounted in a vacuum to eliminate convection heat loss.

ii. **A concentrating or focusing collector:** is one which usually contains reflectors or employs other optical means to concentrate the energy falling on the aperture to a heat exchanger of surface area smaller than the aperture. This type includes:

- Dish type concentrating (Point) collectors: perfectly concentrate sunlight at a focal point.
- Linear concentrating collectors (parabolic trough): linearly concentrate sunlight onto receiver tubes, heating a thermal transfer fluid.

B. Operating Temperature Range: A division can be made between high temperature collectors with a temperature range above 150 °C, medium temperature collectors with a temperature range of 30-150 °C, and low temperature collectors with a temperature range below 30°C. Table 3-6 presents different collector types with their concentration ratio and working temperature range.

C. Mounting: A collector can be mounted to remain stationary, be adjustable so as tilt angle (measured from the horizontal and equivalent to latitude) to follow the change in solar declination or be designed to track the sun. Tracking is done by employing either an equatorial mounting or an azimuth mounting, for the purpose of increasing the absorption of the daily solar radiation. The operation of the tracking mechanism can be either manual or automatic.

D. Types of fluid: A collector will usually use either a liquid or a gas as the transfer fluid. The most common liquids are water or a water- ethylene glycol solution. The most common gas is air.

Table 2-1: Solar collector types

Type of Collector	**Flat Plate Collectors**	**Evacuated Collectors**	**Parabolic trough collectors**	**Parabolic dish collectors**
Concentration Ration	1	1	15-45	100-1000
Typical Working Temperature (^{O}C)	30-80	50-200	80-300	100-500

As shown in Table 2-1, the Parabolic trough collectors provide the desired temperature range to incorporate in DAR machines and therefore is chosen for this study. Parabolic Trough Solar Collector (PTSC), which is also called a cylindrical parabolic collector, employs linear imaging concentration. These collectors comprise of a reflecting surface which resembles a parabolic shape, and a circular cylindrical receiver located along the focal line of the parabola as shown in Figure 2-2.

The cylindrical parabolic reflector focuses all the incident sunlight onto a metallic tubular or flat receiver placed along its length in the focal plane. The heat transfer fluid is allowed to flow through the receiver.

The reflecting surface is mostly made of reflecting mirrors or anodized aluminum sheets. The solar radiations falling on the reflecting surface is concentrated on the focal line of the parabola where a receiver tube carrying the heat transfer fluid is placed. Absorber tube either painted black or electroplated with nickel or chromium in order to increase the absorptivity of the tube. The temperature in this type system can reach as high as 400^{o}C, depending upon the type of reflecting surface, absorber tube materials and heat transfer fluid. A parabolic trough collector system must be positioned in agreement with the sun's position so that it can reflect the incoming beam radiations to the absorber tube.

Concentrating ratio is an important term when talking about concentrating collectors. It is defined as the ratio of the area aperture area of collector and absorber tube's area. Its value ranges from 15 to 45, as presented in Table 2-1. Increase in concentration ratio corresponds to higher working temperatures.

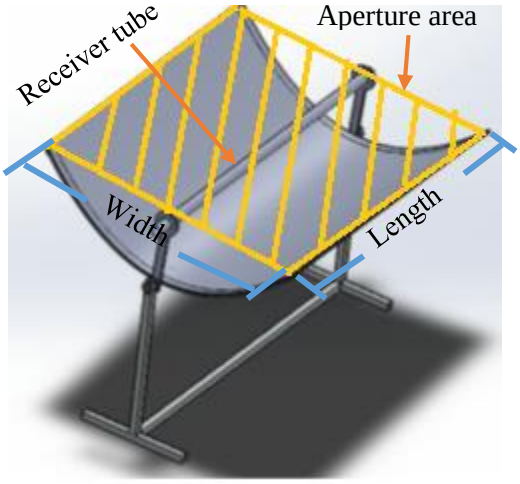

Figure 2-2: Schematic diagram of parabolic trough collector

2.4 Working Fluids Thermodynamic Property Model

The selection of a proper method for estimating the thermodynamic properties of the working fluid is one of the most important steps that can affect the simulation of absorption refrigeration cycles. Therefore, it is important to choose carefully an appropriate method to estimate the different properties of the working fluid. Aspen-Plus includes a large databank of thermodynamic property and transport models with the corresponding mixing rules for estimating mixture properties. Before performing simulations in Aspen-Plus, it is important to ensure which property method is the best reliable thermodynamic model.

(Ben Jemaa et al., 2016) investigates in detail which property model is best used in simulation of DAR cycle using Aspen Plus. To this purpose the predictions of the nine property models available in Aspen-Plus for this mixture are evaluated.

Ammonia/Water mixture has been used as a working pair in absorption refrigeration systems for several decades. Different equations are available in the literatures to determine its thermodynamic properties: Virial equations of state, cubic equations of state, polynomial functions, Helmholtz free energy, Perturbation theory and Gibbs excess energy. Schulz presented a fundamental equation of state for this binary mixture (Mansouri et al., 1996). (Analysis et al., 1987) modified the Schulz's equation of state and developed new correlations for predicting the equilibrium properties required in the analysis of absorption refrigeration cycles. The authors used the Gibbs excess energy equation to determine specific volume, specific entropy and specific enthalpy. The thermodynamic properties can be predicted with the new correlation up to a pressure of

50 bars and a temperature of 500 K. Renon et al. derived an equation of state which can accurately estimate the properties of NH_3/H_2O mixtures. Redlich-Kwong equation of state with two adjustable parameters was used to predict the VLE (vapor-liquid equilibrium) of the working fluid. Ruiter presented a simplified thermodynamic model for the NH_3/H_2O mixture.

The equilibrium pressure and the excess enthalpy of the gas and liquid phases were described using 11 coefficients. Pátekand Klomfar presented five equations to predict VLE properties. The use of these equations avoids iterative procedures when calculating thermodynamic properties of the NH_3/H_2O mixture. The equations were developed by fitting critically assessed experimental data using simple functional forms. The results were presented in the form of an enthalpy concentration diagram. Barhoumi et al. reported a detailed work on the reformulation of the thermodynamic properties of the NH_3/H_2O mixture using the Gibbs energy function. For the liquid phase, a three constant Margules model of the excess free enthalpy was formulated. The vapor phase was considered a perfect mixture of real gases; each pure gas being described by an equation of state. The model developed predicts the thermodynamic properties of the mixture with great accuracy in the three states, i.e. subcooled liquid, superheated vapor and liquid-vapor saturation in the temperature range of 200 to 500 K and a pressure up to 100 bars.

Mejbri and Bellagi modeled the thermodynamic properties of the NH_3/H_2O mixture using three different approaches: An empirical Gibbs free enthalpy model, the Patel-Teja cubic equation of state and the PC-SAFT (Perturbed Chain Statistical Associating Fluid Theory) equation of state. A comparison of these three methods proved the superiority of the PC-SAFT equation of state to predict and extrapolate the thermodynamic properties of the ammonia/water fluid mixture over a larger range of temperature ($273.16 \leq T \leq 613.15$ K) and pressure ($0 < P \leq 210$ bar). Also, the authors recommended the use of the Gibbs free enthalpy model for industrial applications that use NH_3/H_2O as a working fluid at moderate temperatures and pressures, such as absorption refrigeration.

The nine property models implemented in Aspen-Plus and considered for the calculation of the properties of the NH_3/H_2O mixture are listed in Table 2-2. This list includes those called cubic methods (SRK, PR-WS and PR-MHV2, PENG-ROB, PR-

BM, RKS-BM) as well as activity coefficient methods (ENRTL-RK, NRTL-HOC, WILS-RK). The tests of these models were performed by Mansouri in two steps. In the first one, T-x-y VLE predictions of each one of the Aspen-Plus property models are compared with the regressed data reported in for 6 isobars, namely 2, 4, 10, 16, 20 and 25 bars.

Figures 2-3 (a, b, and c) illustrate this comparison at 2, 10 and 25 bars, respectively. It is observed that the maximum equilibrium temperature deviation predicted by the considered nine property models implemented in Aspen-Plus and the data reported by Mejbri and Bellagi was found to be 10^{o}C (Ben Jemaa et al., 2016). In regard to ammonia mass fraction in the liquid phase, the values predicted by the property models SRK, PR-WS and PR-MHV2 are inconsistent in the whole pressure range. This is the case also of the three activity coefficient models (ENRTL-RK, NRTL-HOC, WILS-RK) at 10 and 25 bars, for which the deviations increase with increasing pressure. It is concluded that none of these property models reproduces the ammonia/water vapor-liquid equilibrium data with sufficient accuracy.

Table 2-2: Aspen-Plus thermodynamic property models

No.	Aspen-Plus property model	Model name
1.	ENRTL-RK	Electrolyte NRTL/Redlich-Kwong
2.	RKS-BM	Redlich-Kwong-Soave-Boston-Mathias
3.	PENG-ROB	Standard Peng-Robinson
4.	PR-MHV2	Peng-Robinson Huron-Vidal-Modified
5.	PR-WS	Peng-Robinson-Wong-Sandler
6.	NRTL-HOC	Non-Random-Two-Liquid/Hayden-O'Connell
7.	SRK	Soave-Redlich-Kwong
8.	WILS-RK	Wilson/Redlich-Kwong
9.	PR-BM	Peng-Robinson-Boston-Mathias

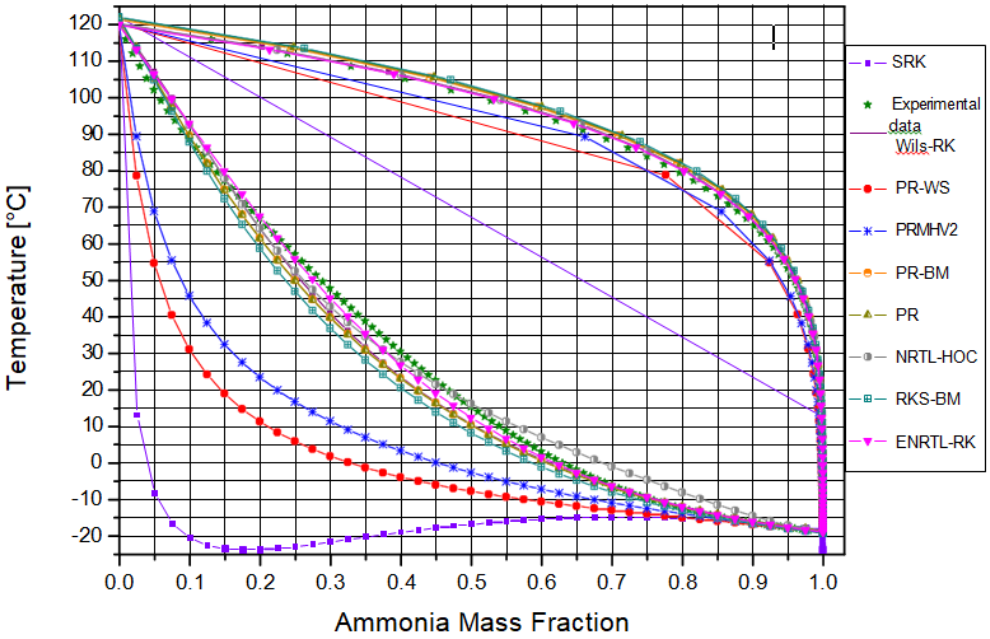

(a) at 2 bars

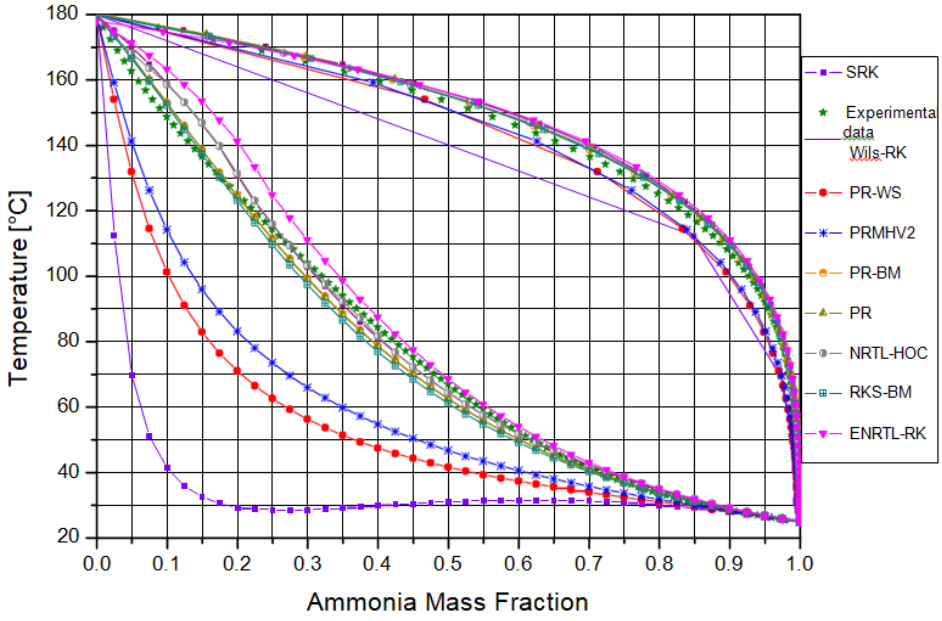

(b) At 10 bars

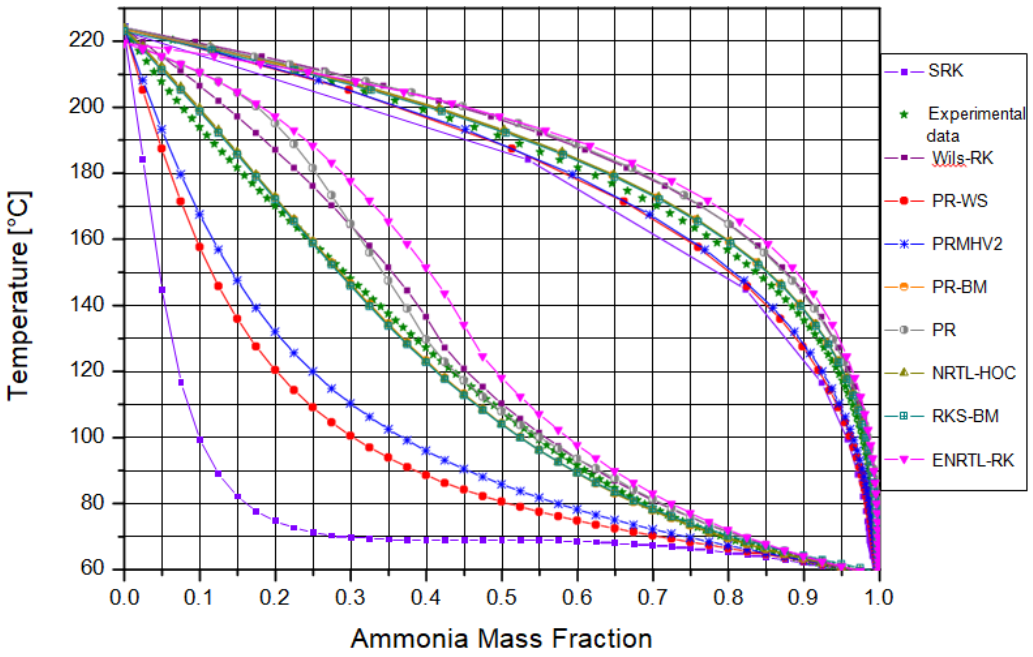

(c) At 25 bars

Figure 2-3 (a, b, c): T-x-y VLE diagram at P = 2 bar, 10 bar and 25 bar respectively for ammonia-water mixture (Ben Jemaa et al., 2016)

Mansouri again predict and extrapolate the thermodynamic properties of ammonia/water fluid mixture over a wide range of temperature ($273.16 \leq T \leq 613.15$ K) and pressure ($0 < P \leq 210$ bar), by evaluating in two steps the nine different models in Aspen-Plus. Firstly, vapor- liquid equilibrium (VLE) calculated by each of the Aspen-Plus property models was compared with the regressed VLE data reported by Mejbri and Bellagi at different pressures. It was concluded that none of these property models predicts the ammonia/water vapor-liquid equilibrium with sufficient accuracy. Secondly, the Aspen Plus data regression tool was used to calculate the parameters of the Aspen Plus property models by fitting the vapor-liquid equilibrium data reported by Mejbri and Bellagi. It was found that the Peng-Robinson-Boston Mathias equation of state (PR-BM) with regressed interaction parameters is the most suitable property model for the water/ammonia fluid mixture in the temperature and pressure ranges encountered in absorption refrigerating machines.

2.5 Diffusion Absorption Refrigeration Cycle

Different researchers reported about DAR which is summarized as shown in the table below. Some of the studies use solar thermal as energy source to drive the generator.

Table 2-3: Literatures reviewed in the area of absorption refrigeration

No.	Title	Method	Main Results	Authors	Year
1	Testing and Simulation of a solar diffusion-absorption refrigeration system for low cost cooling in India	Simulation and Experimental	By reducing the system pressure from 21 bar to 14 bar, a 17% increase in maximum coefficient of performance (COP) is reported, and the system start-up time is reduced by up to 58%.	James Freeman, Ahmad Najjaran, Robert Edwards, Michael Reid, Richard Hall, Alba Ramos, Christos N. Markides	2017
2	Detailed thermodynamic analysis of a diffusion-absorption refrigeration cycle	Mathematical Modelling and Exergy Analysis	A COP of 0.126 associated to a cooling capacity of 22.3W are found. COP is found to exhibit a maximum The COP is found to exhibit a maximum when the heat supplied to the boiler or to the bubble pump is varied.	Ahmed Taieb, Khalifa Mejbri, Ahmed Bellagi	2016

			It is further noted that the COP is very sensitive to the ambient air temperature and to the absorber efficiency.		
3	A new style solar-driven diffusion absorption refrigerator and its operating characteristics	Experimental	The results show that this DAR system can be driven by solar energy to meet the requirements of refrigeration, air conditioning and freezing.	Handong Wanga	2012
4	Numerical and experimental investigation of diffusion absorption refrigeration systems for use with low-temperature heat sources	Numerical and Experimental	The system is charged to 22 bar, and the ammonia mass concentration of the working fluid mixture is 30%. The resulting coefficient of performance (COP) of the system is measured in the range 0.12-0.26.	Ahmad Najjaran, Asmaa A. Harraz, James Freeman, Niall Mac Dowell, and Christos N. Markides	2018
5	Optimum generator temperature to couple different	Simulation	At evaporator temperatures above 5^{o}C with an ambient temperature of 30^{o}C, all solar collector technologies activated different working	A. Acuna, F. Lara, N. Velazquez and J. Cerezo	2014

	diffusion absorption solar cooling systems		mixtures. The optimum coupling temperatures were between 70 and 150^{o}C.		
6	Investigation of Pumping Action of Bubble Pump of Diffusion Absorption Cycles	Numerical simulation	At a fixed bubble pump tube length of 1 m, and ammonia mass fraction of 0.4 and pressure 18 bar at the inlet, numerical results show that, the pumping ration is mostly influences by heat input. Its maximum is directly related by the mass flow rate and tube diameter.	Ali Benhmidene, Khaoula Hidouri & Bechir Chaouachi	2017
7	Diffusion-absorption refrigeration cycle simulations in gPROMS using SAFT-γ Mie	Numerical simulation	The simulation result shows good agreement with other experimental data with a nominal cooling capacity of 100W. In particular, at a charge pressure of 17 bar and when delivering cooling at 5 °C, the model results agree with experimental COP data to within ± 7 % over a range of heat inputs from 150 to 500W. The maximum coefficient of performance (COP) is estimated to be 0.24 at a heat input of 250W.	Asmaa A. Harraza, James Freemana, Kai Wanga, Niall Mac Dowellb, Christos N. Markidesa	2019

8	A numerical investigation of a diffusion-absorption refrigeration cycle based on R124-DMAC mixture for solar cooling	Numerical Simulation	The feasibility of a solar driven DAR using the mixture R124/DMAC as working fluid is investigated by numerical simulation. The results show that the system performance and the lowest evaporation temperature reached are largely dependent upon the absorber efficiency and the driving temperature.	N. Ben Ezzine, R. Garma, A. Bellagi	2010
9	Effect of operating conditions on the performance of the bubble pump of absorption-diffusion refrigeration cycles	Mathematical model	It was found that, the liquid velocity and pumping ratio increase with increasing heat flux, and then it decreases. Optimal heat flux depends namely on tube diameter variations.	Ali Benhmidene, Bechir Chaouachi, Mahmoud Bourouis, And Slimane Gabsi.	2011
10	Modeling of a solar powered absorption cycle for Abu Dhabi	Numerical simulation using TRNSYS	The proposed system was found to consume 47% less electricity than the vapor compression air conditioners. Similar to other solar air conditioners, the proposed system's payback period is long and depends on the cost of the	A. Al-Alili, M.D. Islam, I. Kubo, Y. Hwang, R. Radermacher	2010

			electricity and the design solar fraction. However, the falling costs of solar equipment and the rising costs of fuel and electricity could make these systems more economically sound.		
11	Building and Experimentation of Diffusion Absorption Refrigeration Machines	Experimental	In this experimental case, the value of COP reached was 0.3. Experimental results show that such refrigerator, simply fabricated, gives promising results and could be used for clean and safe use where there is a growing interest.	R. Mbarek, W. Mbarek	2013
12	Experimental Study Of Diffusion Absorption Refrigeration Systems Using Solar Energy	Experimental	Two DAR systems with sub-cooling (DAR1) and without sub-cooling (DAR2) was investigated. DAR1 has achieved its lowest evaporator inlet temperature (-14.8 °C), and DAR2 has reached 0.9°C. COP values of DAR1 and DAR2 are found as 0.2362 and 0.2254.	Engin ÖZBAŞ	2017
13	An approach for modelling the performance of thermal bubble pump.	Mathematical Model	The maximum pumping capacity is found to be independent of the liquid temperature at the inlet to the generator under the assumption of	Ass.Prof. Dr. Abdulwadood Salman Shihab , Dr.	2015

			stable operation of the pump. It is obtained that the slip ratio decreases with the increasing of the submergence ratio and slightly decrease with the decreasing of the tube diameter.	Safaa Hameed Faisal	
14	Investigation of pressure drop in the bubble pump of absorption-diffusion cycles	Numerical	The flow instability is essentially in the two-phase zone, in which the instability is pressure drop type. This instability decreases with increasing the tube diameter and decreasing the heat flux. In the vapor phase, instability is low. It increases with the decreasing of the tube diameter. However, in the liquid phase, flow instability is low too.	Ali Benhmidene, Bechir Chaouachi	2019
15	Numerical and experimental investigation of diffusion absorption refrigeration systems for use with low-temperature heat sources	Numerical and Experimental	The system pressure and condensation temperature are found to be key factors in determining the performance of solar-DAR systems.	Ahmad Najjaran, Asmaa A. Harraz a, James Freeman a, Niall Mac Dowell, Christos N. Markides	2018

16	Modelling and Analysis of Bubble Pump Parameters for Vapor Absorption Refrigeration Systems	Analytical model, Simulation and Experimental	The theoretical model and experimental results showed that the bubble pump liquid mass flow rate varies with all three studied parameters. It was observed that the maximum liquid flow rate of 50g/s (0.11 lbm/s) was achieved at a heat input of 160W (0.22hp), submergence ratio of 0.8, and 10mm of tube diameter.	Julia Aman, Paul Henshaw PhD PEng, David S-K Ting PhD PEng.	2016
17	Simulation of Ammonia-Water Two Phase Flow in Bubble Pump	Simulation	Two flow regimes were distinguished, the first, caused by hydrodynamic effect, its time of oscillation is about 10 s and it decreases with heat flux increasing. In addition, the length of oscillation decreases with heat flux too. For the second regime, it is the steady state regime where liquid velocities and pressure become constant; however, vapor velocities increase in steady regime too.	Jemai Rabeb, Benhmidene Ali, Hidouri Khaoula, Chaouachi Bechir	2017

18	Effect of operating conditions on the performance of the bubble pump of absorption-diffusion refrigeration cycles	Modelling and simulation	The value of heat flux corresponding to the optimal functioning are more influenced by tube diameter (3kW/m^2 for a 4 mm of tube diameter and 5, 10, 13, and 17 kW/m^2, respectively for 6, 8, 10, and 12mm of tube diameter). It increase with tube diameter, but it's weak influenced by varying of inlet pressure or ammonia fraction. It is important to notice that for most significant diameters, the range of heat flux corresponding to maximum pumping ratio is broader. In fact, pumping ratio is slightly influenced by moderate variation of heat flux.	Ali Benhmidene, Bechir Chaouachi, Mahmoud Bourouis, And Slimane Gabsi	2011
19	Thermodynamic analysis of a three-fluid absorption refrigeration machine.	Experimental	With refrigeration capacity measured to be 11W at lowest evaporator temperature, which was obtained at 12.5 bar hydrogen pressure. With a generator power input of 370W the Coefficient of Performance was insignificant.	Andrew Zulu	2000

20	Optimum generator temperature to couple different diffusion absorption solar cooling systems	Mathematical modelling and simulation	At evaporator temperatures above 5^{o}C with an ambient temperature of 30^{o}C, all solar collector technologies activated different working mixtures. The optimum coupling temperatures were between 70^{o}C and 150^{o}C. The global efficiency (COP of the cooling system times efficiency of the solar system) of ETC/NH_3-$LiNO_3$ was between 5 to 54% relatively better than other technologies.	A. Acuna, F. Lara, N. Velazquez, J. Cerezo	2014
21	Modelling and simulation of a solar absorption cooling system for India	Modelling and simulation	Although high reference temperature (temperature of the storage tank) increases the system COP and decreases the surface area of system components, lower reference temperature gives better results for FNP (fraction of total load of non-purchase power) than high reference temperatures do. For this study, a 353K reference temperature was found to be the optimum. The computer program is	V Mittal, K S Kasana, N S Thakur	2006

			also validated by another study made by (LLeri, 1995)		
22	Dynamic testing and modeling of a diffusion absorption refrigeration system	Experimental and Modelling	A generalized model is then proposed by expressing the different model parameters as function of the electric power input. Despite a less good prediction of the evolution of the cooling capacity with time, the general model predicts in a satisfactory manner the cooling capacity of the refrigerator in steady state mode	Radhouane Ben Jemaa, Rami Mansouri, Ahmed Bellagi	2016
23	Dynamic investigation of the diffusion absorption refrigeration system NH_3-H_2O-H_2	Numerical and Experimental	The increase of the average ambient temperature from 23.04°C to 32.56°C causes an increase of the condensation temperature from 29.46°C to 37.51°C, and the best evaporation temperature obtained was 3°C, with an ambient temperature of 23.04°C. The results show that a minimum starting temperature of 152°C and 63.8W electric power are required to initiate the decrease of evaporation temperature.	Mohamed Izzedine Serge Adjibade, Ababacar Thiam, Christophe Awanto, Baye A. Ndiogou, Vincent Sambou	2017

24	Study of a Solar Absorption Refrigeration Machine in the Moroccan Climate	Simulation	The obtained results show that equipping the machine with a distillation column (rectifier) has a great effect in its thermodynamic performances by lowering the operating temperature of the hot source and increasing considerably the solar performance coefficient by 30%	J. Dardoucha, M. Chariaa, A. Bernatchoua, A. Dardouchc, S. Malainea, F. Jeffalid	2019
25	The influence of the evaporator inlet conditions on the performance of a diffusion absorption refrigeration cycle	Numerical Simulation	The temperature at the evaporator inlet has to be as low as possible. In addition, the influence of the purity of the vapor phase at the rectifier outlet on the cycle performance was also studied. It was found that less effort has to be invested in the purification of the hot refrigerant vapor in the rectifier.	Michael Jelinek, Avi Levy, Irene Borde	2016

As mentioned in Table 2-3, (Wang, 2012) made an experimental study on the operating characteristic of a solar driven diffusion absorption refrigeration. (Wang, 2012) presents that a DAR system can be driven by low grade energy resources like solar energy and waste energy to meet refrigeration, air condition and freezing requirements.

(Freeman et al., 2017) made an investigation in diffusion absorption refrigeration system in India's climate and found out that system pressure plays a vital role in the COP as well as the start-up time of the system. The study reported that a reduction of system pressure from 21 bar to 17 bar resulted in an increase of the maximum coefficient of performance by 17% and reduction of the start-up time by 58%. This shows that an optimum total system pressure is crucial to obtain the best result from diffusion absorption refrigeration systems.

(Taieb et al., 2016) examines a thorough mathematical modeling and exergy analysis of diffusion absorption refrigeration system of a 22.3W cooling capacity. (Taieb et al., 2016) found the the COP to be 0.126 and describes that the COP is very sensitive to the heat input to the generator, the ambient temperature and the absorber efficiency. The study made by (Ben Ezzine et al., 2010) reinforces this finding. (Ben Ezzine et al., 2010) explains using numerical investigation of solar powered DAR system that the overall system performance and the minimum evaporative temperature that can be achieved are greatly dependent on the driving temperature from the solar collectors and the efficiency of the absorber.

(Najjaran et al., 2018) reports a numerical and experimental investigation of diffusion absorption system using a low temperature heat source to heat the generator. The diffusion absorption refrigeration system operating under total system pressure of 22 bar with ammonia mass concentration of the working fluid at 30%, shows a coefficient of performance (COP) in the range of 0.12 to 0.26.

Another important factor in diffusion absorption refrigeration system is the efficiency of the bubble pump. (Benhmidene et al., 2017) investigates a bubble pump length of 1 m, at system pressure of 18 bar and ammonia mass concentration fraction of 0.4. (Benhmidene et al., 2017) found that the pumping action is highly influenced by the heat input to the generator part of the bubble pump. (Benhmidene et al., 2017) also found out that the maximum pumping action is directly related to the mass flow rate of the working fluid being pumped and tube diameter of the bubble pump.

Other simulation studies are also done in the area of diffusion absorption refrigeration. (Harraz et al., 2019) uses SAFT-γ Mie in gPROMS software to validate a 100W cooling capacity diffusion absorption system at system pressure of 17bar and evaporative temperature of 5^{o}C. The results obtained from the model agrees with experimental coefficient of performance data within ±7% over generator heat input of 150-500W. (Harraz et al., 2019) also reports the maximum COP at 250W heat input to be 0.24.

Other simulation studies include the use of different working fluid pairs. (Ben Ezzine et al., 2010) investigates the use of R124/DMAC *(Tetrafluoroethane /Dimethylacetamide)* for solar powered diffusion absorption refrigeration cycle. (Ben Ezzine et al., 2010) found out that the system performance and the minimum evaporative temperature that can be achieved are greatly dependent on the driving temperature from the solar collectors and the efficiency of the absorber.

(Benhmidene et al., 2011) presents a mathematical model that describes the effect of operating conditions on bubble pump performance of diffusion absorption refrigeration. (Benhmidene et al., 2011) found that the working fluid velocity and pumping ratio increase with increasing heat flux and the it decreases. It also found that the optimum heat flux depends primarily on the tube diameter of the bubble pump. This means there is an optimal heat flux that corresponds to a specific tube diameter.

(Al-Alili et al., 2012) studies a solar driven absorption cycle in Abu Dhabi region. A solar powered absorption model was proposed and the transient performance of the model was performed using TRANSYS. The proposed system is found to consume 47% less electricity than vapor compression cycle. (Al-Alili et al., 2012) also studies the economic feasibility of the system. The study shows that the payback time of the system is relatively longer compared to the conventional systems. However, the reduction trend in the solar equipment and the rising cost of fuel and electricity could make the system more economical in near future.

(Mbarek & Mbarek, 2013) reports design and experimentation of n-butane/octane (C_4H_{10}/C_8H_{18}) diffusion absorption cooling machine using He as an auxiliary gas for air conditioning purpose, with a cooling capacity of 55W. The result shows a good performance and a relatively higher COP of 0.3. This is probably due to the use of a different kind of working fluids.

(Özbaş, 2018) presents an experimental investigation of two solar types of solar powered absorption refrigeration systems. One with sub cooling of liquid ammonia entering the evaporator and the other without sub cooling. The results show that the DAR system with sub cooling yielded lower evaporator temperature and a better COP of 0.2362 while the DAR system without sub cooling yielded a COP of 0.2254 but produced longer cooling time.

(Shihab & Faisal, 2015) developed a mathematical model to study the effect of different parameters on the performance of the thermal bubble pump. The study employs the one dimensional slug flow model in order to describe the void fraction in the riser tube and adopts a method to evaluate the two-phase frictional pressure drop. (Shihab & Faisal, 2015) also includes an experimental observation of three different sized tubes with three different submergence ratios using water as a working fluid. The results indicate that increasing the submergence ratio and the riser diameter increases the pumping capacity at constant riser length. On the other hand, the slip ratio decreases considerably with increasing the submergence ratio and slightly decreases using with decreasing riser diameter. The maximum pumping capacity was also found to be independent of the temperature of the liquid at the generator inlet.

(Ting & Aman, 2016) made a similar study to predict the performance of a bubble pump by varying the heat input at the generator to different sized riser tubes with varying submergence ratio. The study reports both theoretical and experimental analysis to be in close agreement. (Ting & Aman, 2016) found out that the liquid mass flow rate varied with each parameter under observation. A maximum liquid flow rate of 50g/s was recorded at a heat input of 160W, submergence ratio of 0.8 and 10mm riser diameter.

(Rabeb et al., 2017) examines the effect of instability in the bubble pump efficiency. By Considering two-phase flow and using a drift flow model, it develops mathematical equation for resolving hydrodynamic parameters like void pressure, liquid and vapor velocities. The model uses ammonia-water as a working fluid, where mass fraction of ammonia is 0.6. For the simulation purpose a heating flux of 2 kW/m^2 to kW/m^2 and a riser length of 1m with 2.5mm of diameter is used. The results show that liquid and vapor velocities oscillate with time. However, void fraction remains steady. (Rabeb et al., 2017) identifies two regimes, the first caused by hydrodynamic effect, its time of oscillation is found to be 10 seconds, but decreases with heat flux increasing. A

reduction in length of time of oscillation as heat flux increases was also observed. The other regime is the steady state regime where the liquid velocities and pressure remain constant; however, vapor velocities show increment in steady state regime as well. The study also points out that pressure drop oscillation increasing heat flux and time.

A similar study presented in (Benhmidene et al., 2011) studies the influence of the heat input and operating conditions on the flow characteristic in the thermal bubble pump of diffusion absorption cycle. It uses two-fluid model for the two-phase flow region of ammonia-water mixing, considering the hydrodynamic non-equilibrium between the liquid and vapor phases. The results show that vapor velocity varies linearly with heat flux, whereas the liquid velocity and the pumping rate show a maximum value that depend on operating conditions. The value of heat flux corresponding to the optimal functioning of the bubble pump or maximum pumping ratio are greatly influenced by tube diameter (3kW/m^2 for a 4mm of tube diameter and 5, 10, 13, and 17 kW/m^2, respectively for 6, 8, 10, and 12mm of tube diameter). It increases with tube diameter, but it's slightly influenced by varying of inlet generator pressure or ammonia fraction.

(Zulu, 2000) made a thermodynamic analysis of a three-fluid absorption cycle. The analyzed data in the form of temperatures, hydrogen pressure and power input revealed that the time-temperature response of the unit improved from six hours (according to manufacturer's recommendations) to just over one hour. This data was recorded for a range of hydrogen pressures between 7.5 bar and 27.5 bar and for power supplies of 261W, 315W and 370W. Despite the much faster time response, the performance of the unit was poor. The refrigeration capacity was measured to be 11W at lowest evaporator temperature, which was obtained at 12.5 bar hydrogen pressure. With a generator power input of 370W the Coefficient of Performance was insignificant.

(Acuña et al., 2014) presents the study of the generator temperatures to achieve the highest efficiency in different solar diffusion absorption cooling systems. Ammonia-lithium nitrate (NH_3-LiNO3) and sodium ammonia-thiocyanate (NH_3-NaSCN) were examined as the working mixtures, and the flat-plate collector (FPC), the flat-plate collector improved (FPCI), the evacuated-tube collector (ETC) and the compound parabolic concentrator (CPC) were the thermal energy sources. The study was conducted with a simulation in steady-state conditions. The effects of the generator temperature on the global efficiency of each solar cooling system were studied. The

results indicate that the FPC and the FPCI cannot activate the cooling system at evaporator temperatures below 0^{o}C and the ambient temperature is at 40^{o}C. At evaporator temperatures above 5^{o}C with an ambient temperature of 30^{o}C, all solar collector technologies activated different working mixtures. The global efficiency (COP of the cooling system times efficiency of the solar system) of ETC/NH_3-$LiNO_3$ was between 5 and 54% relatively better than other technologies.

(Mittal et al., 2006) performed a modelling of a solar-powered, single stage, absorption cooling system with storage tank. The model uses a flat plate collector and water–lithium bromide as a working fluid. A computer program has been developed for the absorption system to simulate various cycle configurations with the help of various weather data for a village in India. (Mittal et al., 2006) primarily studies the effects of hot water inlet temperatures on the coefficient of performance and the surface area of the absorption cooling component. The results show two main findings. One, the hot water inlet temperature is found to affect the surface area of some of the system components. Increasing this temperature decreases the absorber and solution heat exchanger surface area, while the dimensions of the other components remain unchanged. And two, although high reference temperature (temperature of the storage tank) increases the system COP and decreases the surface area of system components, lower reference temperature gives better results for FNP (fraction of total load of non-purchase power, FNP = 1 - Q_{aux}/Q_{load}) than high reference temperatures do. For this study, a 353 K reference temperature was found to be the optimum. The computer program is also validated by another study made by (Ileri, 1995)

(Ben Jemaa et al., 2016) describes experimental investigation and a consequent appropriate dynamic modeling of a commercial DAR that operates by an electric heater. The experimental results were used to propose an appropriate model that can be used to predict the transient behavior of the commercial DAR. (Ben Jemaa et al., 2016) used a Black box model approach in order to describe the relationship between the heat input and the cooling output of the system. In its study the transfer function of a first order with delay was found to be adequate for all applied heat inputs. Based on the different model parameters, a generalized model of the system is then proposed. The generalized model is found to predict the steady state of the machine with good satisfactory with maximum deviation of 7.1%. While the initial transient (evolution of the cooling

capacity at the start) was found to be less accurately predicted. The proposed model can be used to predict the behavior of other commercially available DAR machines.

(Adjibade et al., 2017) discusses a transient investigation of a DAR cycle that uses ammonia-water-hydrogen as working fluids, by applying numerical and experimental methods. The study develops a dynamic model for each components of the system and solve numerically using MATLAB and EES in order to predict the transient performance of the system. The focus of the study is in the temperature profile of each component. The results show that an increase in ambient temperature causes an increase in condensation temperature, as expected. And the minimum evaporation temperature obtained was 3^oC at a generator temperature of 152^oC. The results were later validated with an experimental investigation.

(Dardouch et al., 2019) examines the performance of solar operated absorption refrigeration machine in Morocco climate. The study uses a real metrological climate data as an input and a FORTRAN program to simulate and compare the performance of the absorption system. (Dardouch et al., 2019) makes a comparison between an absorption system that is equipped with a distillation column with one that does not. A distillation column purifies the outgoing ammonia vapor from the generator by condensing and trapping the water vapor before it enters the condenser. The results show that the cycle that is integrated with a distillation column showed a better thermodynamic performance by reducing the hot source temperature while maintaining the cooling capacity. Consequently, the COP was found to increase by 30%. This allows the use of cheap solar collectors, like flat plate collectors, to drive the system.

However, the study made by (Jelinek et al., 2016) rather shows a different result. (Jelinek et al., 2016) investigates numerically the effect of the purity of the refrigerant vapor at the exit of the rectifier. Interestingly, (Jelinek et al., 2016) found out that as purity of refrigerant vapor entering the condenser reduces, the amount of heat supplied to the generator reduces while the Q_{evp} remains the same. Thus, increasing the COP. This is because, even though the heat rejected by the rectifier decreases, the heat rejected by the condenser increases and the heat supplied by the generator decreases. The research made by (Starace et al, 2012) confirms this result.

In addition, (Jelinek et al., 2016) examines three sub-cooling configurations numerically: no sub-cooling, partial sub-cooling and full sub-cooling. The sub-cooling

is done after the refrigerant leaves the condenser and before it enters the evaporator. The partial sub-cooling is done only by the refrigerant heat exchanger while full sub cooling is done by both the refrigerant heat exchanger and the evaporator. It was discovered that for the same heat input, the partial sub-cooling produces the best cooling effect and the highest COP.

In general, several researches have been conducted on diffusion absorption cooling systems, however, most of these studies were experimental investigations, and very few studies focused on solar thermal powered cooling systems. Most of the studies did not consider detailed parametric study that can predict the operation of the system.

In order to improve the system design of a solar powered DAR system, a parametric study must be carried out to investigate the influence of key parameters on the overall system performance. If experiments were used to perform the parametric study, effects of one key parameter on the overall system performance would normally require several cooling seasons and hence years to establish a conclusion. In addition, it is also difficult to keep the performance of the system components constant over the entire experimental period as the components deteriorate with time. Thus, it is extremely difficult and expensive to carry out experiments to investigate the influence of all the key parameters on the overall system performance of a solar powered DAR system. The objective of this study is therefore to model a complete DAR system that uses NH_3–H_2O-H_2 as a working fluid in order to perform de4tailed parametric study.

3 METHOD AND METHODOLOGY

In this chapter, the methods and methodologies incorporated in the study are presented in detail. Choosing appropriate simulation tool and thermodynamic property models of working fluids are keys to achieving realistic and acceptable results. Simulated components of the DAR system are modeled to represent real components as much as possible in order to avoid unrealistic outputs. The following flow chart shows the steps used followed in reaching the results obtained.

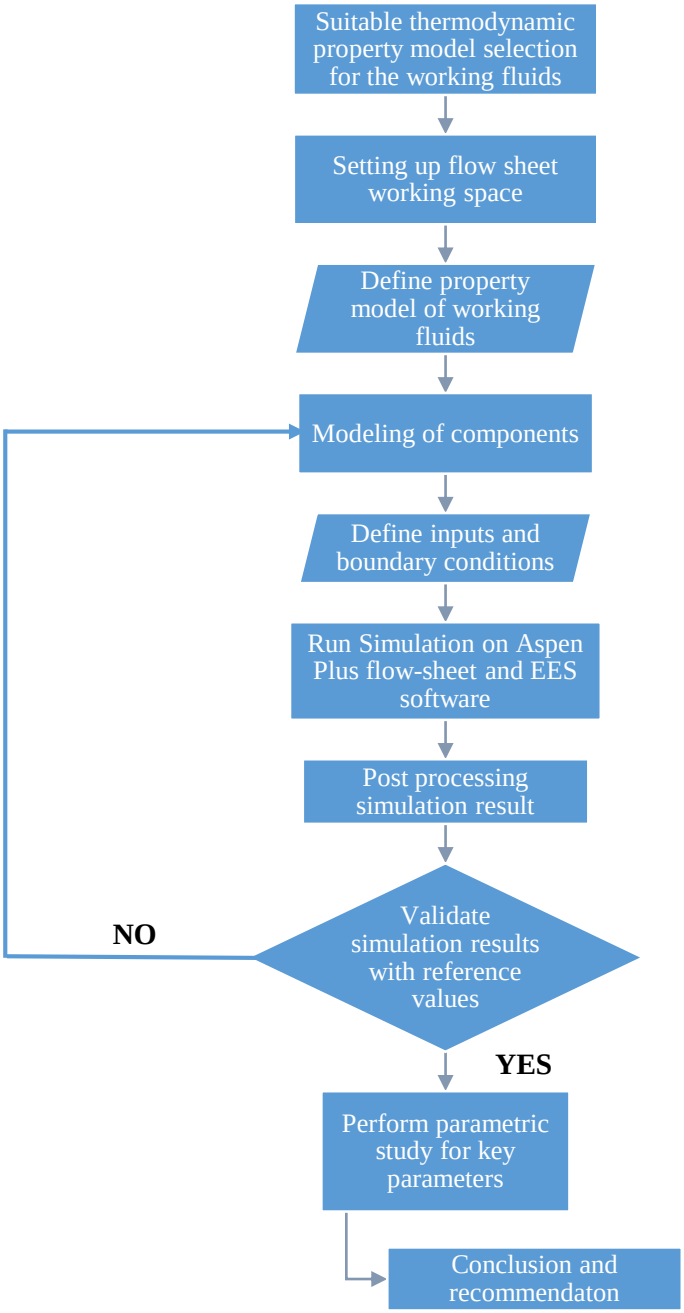

Figure 3-1: Methodology flowchart

3.1 The Choice of Simulation Tool

There are various process modeling and simulation tools that are commercially available. Among them are MATLAB, TRNSYS, DWSIM, EES and ASPEN PLUS.

Aspen Plus is a process flow sheet simulator. A flow sheet simulator is computer software that is used to quantitatively model a chemical process (Ojha et al., 2020). Aspen Plus is a tool that can be used to tackle different chemical process, in the form of modeling, simulation, optimization, data regression, design specifications, and sensitivity analysis. Different property models and thermodynamic properties of pure and mixture substances are built into the software, making it possible to solve complex system processes with binary or tertiary mixture. Similar studies performed using this tool include, optimization of refrigerant by (He & Lin, 2020), theoretical and experimental study of absorption and absorption/diffusion refrigerating machines by (Mansouri et al., 1996), and modelling absorption chiller by (C. Somers et al, 2014).

3.2 Selection of Working Fluids

There are several possible absorbent–refrigerant working pairs that can be used in absorption refrigeration systems. The choice should be made carefully, since the performance of the system differs according to the chosen working pair (Chauhan et al., 2022). The proper selection depends on the maximum temperature of the heat source, the desired characteristics of the refrigeration system, the properties of the working pair constituents and the affinity between them (which depend on the chemical, physical and thermodynamic properties of the substances); and even their cost, availability and environmental impact is also considered when selection is made.

3.2.1 Refrigerant

Regarding the pure refrigerant, the following properties are the design target:

1. Low boiling point at atmospheric pressure
2. High latent heat of vaporization
3. Low heat of mixing with the absorbent
4. Low viscosity
5. The normal boiling point and the vapor pressure of the refrigerant should not be close to those of the absorbent to allow easy separation and regeneration by heating.

3.2.2 Absorbents

Regarding the pure absorbent, the following properties are the design target:

1. High boiling point at atmospheric pressure Compare to refrigerant.
2. Stability and non-toxicity.
3. Low heat of mixing with the refrigerant.
4. Non- Corrosively and mutual solubility with refrigerant.
5. Normal boiling points above 100°C should satisfy the low volatility requirement of the absorbent.

3.2.3 Refrigerant- Absorbents mixture

Regarding the mixture, the properties to be considered are as follows:

1. The boiling point of the solution is in a range that can be provided by low-quality heat sources.
2. High miscibility between the refrigerant and the absorbent. It is a necessity to have a completely miscible solution to have a homogeneous solution in the vapor and liquid phases under all conditions.
3. Low heat of mixing
4. No solid formation under operation conditions.

Many working fluids are suggested in literature. A survey of absorption fluids provided by (Shankar Ganesh & Srinivas, 2011) suggests that, there are some 40 refrigerant compounds and 200 absorbent compounds available. A summary of the possible working pairs for absorption systems is shown in Table 3-1 and some of working pairs are described below:

Table 3-1: Summary of some working pairs for absorption systems

Refrigerant	Possible absorbents
H_2O	Salts / Alkali halides / LiBr / Ionic liquid / $LiClO_3$ / LiBr based multi-component salt mixtures (LiBr + single salt, LiBr + binary salt systems, LiBr + ternary salt system) / $CaCl_2$ / $ZnCl_2$ / ZnBr / Alkali nitrates / Alkali thiocyanates / Bases Alkali hydroxides / Acids / H_2SO_4 / H_3PO4.

NH_3	H_2O / $LiNO_3$ / $LiNO_3$ + H_2O / Alkali / Sodium- Thiocynatc (NaSCN) / Ionic liquid / $MnCl_2.CaCl_2$
TEF	NMP / E181 (TEGDME) / DMF / TEG / DMETEG / DWA /BZL / QUN / Pyrrolidone / H_2O
HFC(R12,R21,R25, R22, R134, R134a,….)	DMAC / DMF / DMETEG / Ionic liquid / NMP / MCL / DMEU
Methanol	H_2O / Ionic liquid / LiCl / LiBr / LiI / $ZnBr_2$ / $ZnCl_2$ / $LiBr.ZnBr_2$ / $LiI. ZnBr_2$ / H_2O. LiBr / LiSCN / LiCl. LiBr
Butane	Ocetone / ethanol
Ethanol	H_2O / LiCl / LiBr / LiI / $ZnBr_2$ / $ZnCl_2$ / $LiBr.ZnBr_2$ / Tri and Diethylene glycol
MDEA(methyl diethyl amine)	H_2O
n- propanol	LiCl / LiBr / $ZnBr_2$ / $ZnCl_2$
Methyl chloride	DME / TEG

The most common working Fluid are LiBr-H_2O where Water is the refrigerant and LiBr is the absorbent and H_2O-NH_3 are widely used in absorption systems where Ammonia (NH_3) is refrigerant and Water (H_2O) is the absorbent (Alazazmeh & Mokheimer, 2015). The higher boiling point of water compared to ammonia means that LiBr-H_2O systems are typically used in cooling applications that require temperatures greater than 5°C, and is mostly used for air-conditioning applications rather than for food chilling. On the other hand, H_2O-NH_3 systems have a far wider cooling temperature range, ranging from -60°C to +10°C. LiBr-H_2O systems require lower working pressures with higher heat source temperatures, making them more suitable than H_2O-NH_3 for systems with multiple-stage heat addition (Najjaran et al., 2018). The advantages and disadvantages of the two most common working fluids is summarized in the following Table 3-2.

Table 3-2: Advantages and disadvantages of the two most common working fluid pairs.

Working pair	Advantage	Disadvantages
$NH_3 – H_2O$	• Used where lower temperature is required. • In nature, ammonia is produced by biological processes, is naturally decomposed, and does not add to the global greenhouse effect. • Ammonia is readily soluble in water. • The odor of ammonia has a highly alerting effect. Refrigerant leaks are therefore detected at once. • NH_3 has a high latent heat of vaporization. • NH_3 and water are highly stable for a wide range of operating temperature and pressure. • Water/NH_3 is environmentally friendly and low cost.	• the freezing point of NH_3 is - 77°C. Since both NH_3 and water are volatile, the cycle requires a rectifier to strip away water that normally evaporates with NH_3. • NH_3 is toxicity. • NH_3 is corrosive action to many metals.
LiBr - H_2O	• LiBr/water are non-volatility absorbent of LiBr (the need of a rectifier is eliminated). • high heat of vaporization of water. • Low toxicity.	• At high concentrations, the solution is prone to crystallization. • Corrosive to some metal • Expensive. • Water as a refrigerant

	limits the low temperature application to that above 0°C. • As water is the refrigerant, the system must be operated under vacuum conditions.

Many other researches have been carried out to investigate the thermodynamic properties of different working fluid like fluorocarbon refrigerant with number of organic solvents. However, more studies are still needed to make them commercially viable. For this research work, ammonia-water was used because of its commendable performance in absorption system for low generation temperature, evaporative temperature and total system pressure.

3.3 Selection of Thermodynamic Property

From reviewing literatures in section 2.4, it is concluded that simulations on Aspen-Plus flow-sheeting software of absorption refrigerating machines working with NH_3/H_2O fluid mixture should be done using the **Peng-Robinson-Boston-Mathias equation of state (PR-BM)**, with fitted parameters, as a property model to gain the most reliable result.

3.4 System Configuration

Figure 3.2 below shows a schematic representation of the diffusion-absorption refrigerator investigated. Material streams connecting the various components of the refrigerator are identified by state points.

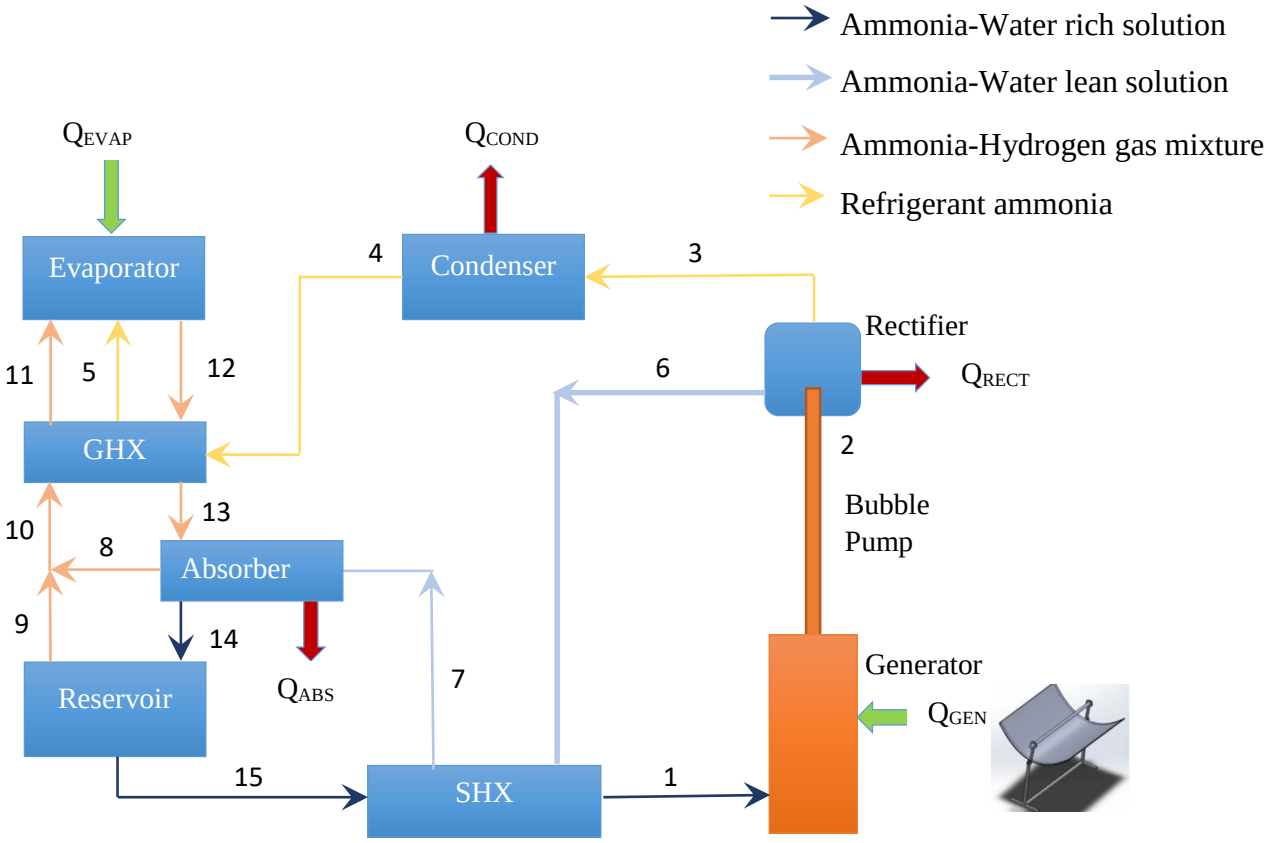

Figure 3-2: Shows the key processes in a typical DAR system using ammonia-water and hydrogen as the auxiliary gas

In above Figure 3-2, refrigerant-rich solution (1) receives heat (Q_{GEN}) in the generator by a solar thermal system, where it boils in the bubble pump. The rising refrigerant bubbles lift the solution through the bubble-pump's inner tube. At the end of this tube (2), the vapor refrigerant separates from the refrigerant-weak solution. Because of the relatively volatile water absorbent, the ascending vapor refrigerant is not pure enough to proceed directly to the condenser, thus more refrigerant should be rectified emitting heat (Q_{RECT}) to the ambient. The refrigerant-weak solution and reflux liquid flow down the bubble pump shell. While the rectified near pure vapor refrigerant (3) enters the condenser rejecting heat (Q_{COND}) to the ambient and exiting in a liquid state (4). After being sub-cooled through a gas heat exchanger, the near pure refrigerant (5) evaporates into the auxiliary gas (11) coming from the absorber and passed through the gas heat exchanger taking in heat (Q_{EVAP}) from the cold space. The refrigerant partial pressure develops and the partial pressure of the auxiliary gas reduces, as it passes through the evaporator according to Dalton's Law. The refrigerant-auxiliary gas mixture leaving the evaporator (12) flows into the reservoir (solution tank) before entering the absorber

(13), Meanwhile the weak refrigerant solution that separated at the bubble pump (6) comes to the absorber passing through a solution heat exchanger, where it contacts the refrigerant-auxiliary gas mixture, flowing counter-currently. There the absorption of the refrigerant into the solution is accompanied by a heat rejection (Q_{ABS}), while the incondensable auxiliary gas ascends the absorber (8) and returns to the evaporator via the gas heat exchanger. The rich solution exiting the absorber (14) gets into a reservoir where any remaining auxiliary gas is separated (9) and sent to the gas heat exchanger. While at the bottom the rich solution leaves the reservoir, passes through a solution heat exchanger and enters the generator, continuing the cycle.

The initial assumptions of the state points for the refrigerator simulation are summarized in Table 3-3.

Table 3-3: State point assumptions for the DAR simulation.

State point	Assumption
2	Determined by the generator model
3	Determined by the rectifier model
4	Determined by the condenser model
13	Determined by gas heat exchanger model
12	Determined by the evaporator model
10	Determined by the absorber and solution tank/reservoir model
14	Determined by the absorber model
5, 11	Determined by gas heat exchanger model
15	Determined by the solution tank model
6	Determined by the generator, bubble pump and rectifier model

3.5 Thermal Modeling and Governing Equations

The thermodynamic analysis of vapor absorption cycle is based on the following three governing equations.

i. Mass balance $\Sigma m = 0$
ii. Material balance (or ammonia mass balance) $\Sigma mx = 0$
iii. Energy balance $\Sigma Q = 0$

The mass, ammonia mass balance, and energy balance equations for various components of the diffusion absorption refrigeration cycle are presented below.

3.5.1 Generator and Bubble Pump as Unit

For simplification of balancing, generator and bubble pump are combined into a single unit. The rich solution that is heated in the generator comes from state point 1. Vapors of ammonia and water are produced and rise to rectifier through the bubble pump.

General mass balance equation:

$$m_1 = m_2 \quad (3.1)$$

Ammonia mass balance equation:

$$m_1 x_1 = m_2 y_2 \quad (3.2)$$

Energy balance equation:

$$Q_{gen} = m_1 h_1 - m_2 h_2 \quad (3.3)$$

3.5.2 Rectifier

The rectifier has the gaseous ammonia–water solution at 2 being cooled to produce almost pure ammonia refrigerant at state 3 and weak solution at state 6 that returns back to the absorber through the solution heat exchanger. Thus, energy balance equation for rectifier gives the heat rejection from the rectifier as:

General mass balance equation:

$$m_2 = m_3 + m_6 \quad (3.4)$$

Where $m_1 = m_2$

Ammonia mass balance equation:

$$m_2 y_2 = m_3 y_3 + m_6 x_6 \quad (3.5)$$

Energy balance equation:

$$Q_{gen} = m_2 h_2 - m_3 h_3 - m_6 h_6 \quad (3.6)$$

3.5.3 Condenser

Ammonia vapor after leaving the rectifier at state 3 condenses by rejecting heat into the atmosphere. Ammonia is condensed in the condenser at constant pressure in the condenser.

General mass balance equation:

$$m_3 = m_4 \quad (3.7)$$

Ammonia mass balance equation:

$$m_3 y_3 = m_4 x_4 \quad (3.8)$$

Thus, heat rejected at the condenser can be written as:

$$Q_{cond} = m_3 h_3 - m_4 h_4 \quad (3.9)$$

The condensed refrigerant liquid at state 4 is coming from the condenser and flows into the evaporator through gas heat exchanger.

3.5.4 Evaporator and Gas Heat Exchanger

Subcooled liquid ammonia at state 5 mixes with inert gas with some ammonia residual gas from state 11. This causes pressure of both of ammonia liquid and hydrogen gas to drop, and mixtures of ammonia and hydrogen gas with their respective partial pressures flow through the evaporator to state 12.

General mass balance equation:

$$m_{12} = m_5 + m_{11} \quad (3.10)$$

$$m_{12} = m_{13} \quad (3.11)$$

$$m_{10} = m_{11} \quad (3.12)$$

$$m_4 = m_5 \quad (3.13)$$

Ammonia mass balance equation:

$$m_{12} y_{12} = m_5 x_5 + m_{11} y_{11} \quad (3.14)$$

$$m_{12} y_{12} = m_{13} y_{13} \quad (3.15)$$

Energy balance equation:

$$Q_{evap} = m_{11} h_{11} + m_{H_2} C_{p,H_2} T_{11} + m_5 h_5 - m_{12} h_{12} - m_{H_2} C_{p,H_2} T_{12} \quad (3.16)$$

3.5.5 Absorber and Reservoir

Ammonia and hydrogen gas mixture at state 13 and the lean solution coming from the solution heat exchanger state 7 enters the absorber. Ammonia vapor is readily absorbed into the weak ammonia solution to produce strong ammonia solution and pass to the reservoir at state 14. During the absorption processes, hydrogen gas is first liberated in

the absorber and leaves at state 8. After that some hydrogen that passed to the reservoir with the strong solution is again liberated and leaves the r which leaves the receiver tank along with some amount of unabsorbed ammonia gas. Thus, residual gas mixture (hydrogen and unabsorbed ammonia) leaves the receiver tank and moves towards gas heat exchanger.

General mass balance equation:

$$m_{13} + m_7 = m_{10} + m_{15} \quad 3.17$$

Ammonia mass balance equation:

$$m_{13}y_{13} + m_7x_7 = m_{10}y_{10} + m_{15}x_{15} \quad 3.18$$

Energy balance equation:

$$Q_{abs} = m_{13}h_{13} + m_{H_2}C_{P,H_2}T_{13} + m_7h_7 - m_{10}h_{10} - m_{H_2}C_{P,H_2}T_{10} - m_{15}h_{15} \quad 3.19$$

Heat of absorption is liberated when ammonia is absorbed in weak solution. Due to this, temperature of leaving strong solution and inside gas increases. Also heat is rejected from the absorber into the atmosphere.

3.5.6 Solution Heat Exchanger

In solution heat exchanger, strong solution is heated from state 15 to state 1 by extracting heat from the weak solution which returns from the rectifier.

Mass balance for lean solution:

$$m_6 = m_7 \quad 3.20$$

Mass balance for rich solution:

$$m_1 = m_{15} \quad 3.21$$

Ammonia mass balance for lean solution:

$$x_6 = x_7 \quad 3.22$$

Ammonia mass balance for rich solution:

$$x_1 = x_{15} \quad 3.23$$

Energy balance equation:

$$m_6 h_6 + m_{15} h_{15} = m_1 h_1 + m_7 h_7 \quad 3.24$$

The partial pressure of NH_3 in the gas mixture is defined as:

$$\frac{P_{partial}}{P_{total}} = \frac{N_{NH_3}}{N_{NH_3} + N_{H_2}} \quad 3.25$$

where N is the number of moles.

For solving the thermodynamic equations, properties of the ammonia–water solutions at different state points in the cycle are needed. These properties of the working fluid and gas mixture at different pinch points are calculated by Aspen Plus using a thermodynamic model. The thermodynamic model applied is discussed in detail in section 3.7. The corresponding results at the state points are also checked using EES.

3.6 Components Modeling and Input Data

This section describes the models used to define each component in Aspen Plus. The "Break point" approach is applied to simulate the absorption cooling cycles to develop the refrigerator model. The theoretical model predictions were later compared with reference data to determine their accuracy.

The development of a running model for a diffusion-absorption refrigerator in the Aspen-Plus environment is based on the appropriate selection of the equivalent blocks for the main components of the refrigerator. The models used for the components of the DAR machine simulated are presented in Table 3-4.

Table 3-4: Summery of Aspen-Plus blocks used for the DAR components

Component	Aspen-Plus Block Type Name	Block Representation
Condenser	Heater	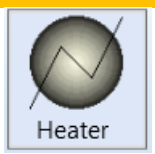
Evaporator	Heater	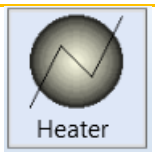
	Mixer	

Absorber	RadFrac (Absorber)	
Solution Heat Exchanger	HEATX (Two-flow heat exchanger)	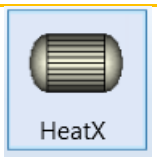
Generator	RadFrac (STRIP)	
Rectifier	RadFrac	
Solution Tank	Flash	
	Mixer	
Gas Heat Exchanger	MHeatX (Three-flow heat exchanger)	
Bubble Pump	Flash	
	Heater	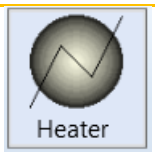

The Aspen-Plus model developed for the diffusion-absorption refrigerator is shown in the following Figure 3-3. Tables 3-5 summarize the refrigerator's components and their corresponding input data, respectively.

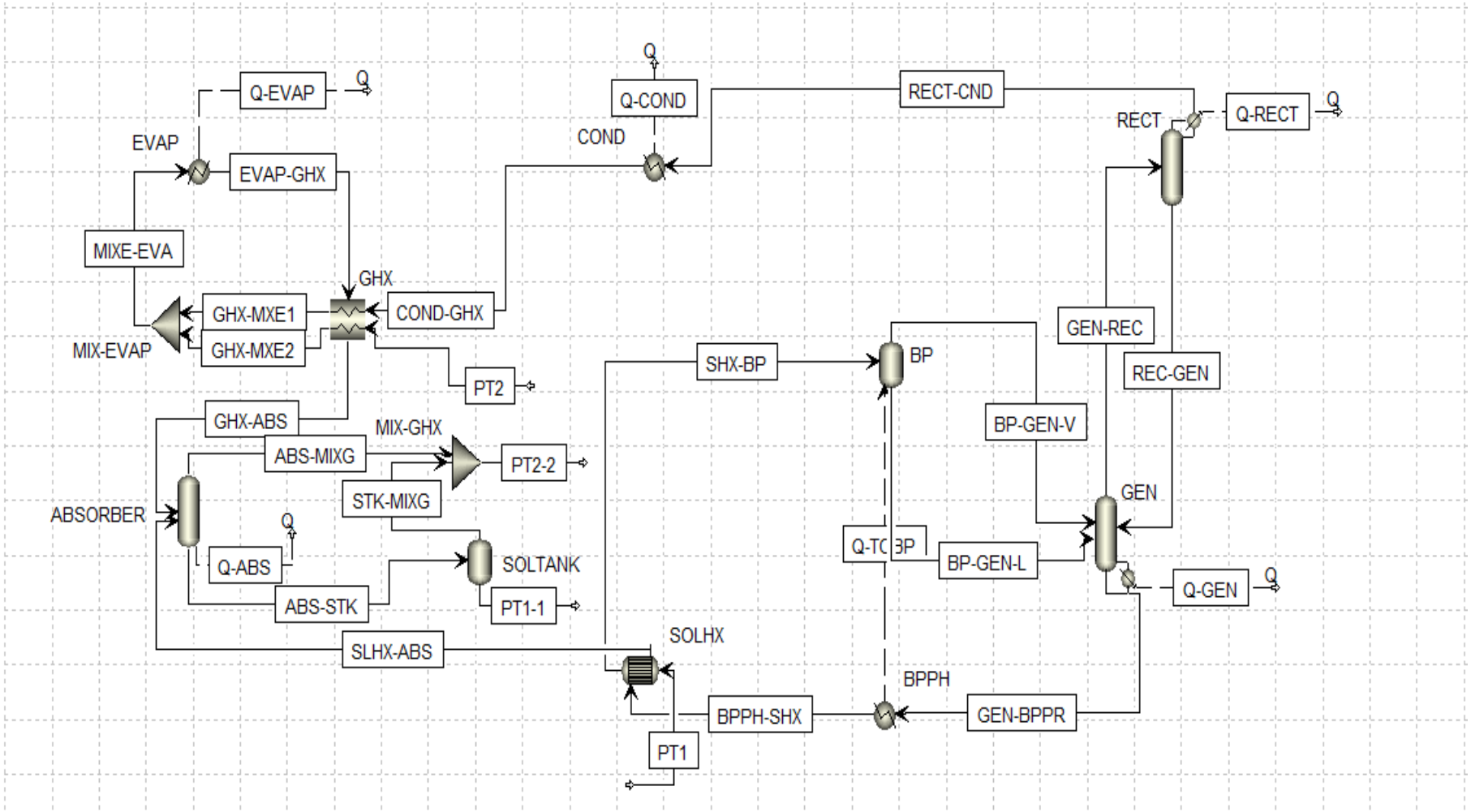

Figure 3-3: Aspen Plus DAR model

Table 3-5: Initial input parameters used in the models of the DAR components.

Block	Input
Solution Heat Exchanger	Cold stream outlet temperature, 150°C
Generator	Heat duty = 50W
Rectifier	Distillate mass rate, 0.06 kg/h
Condenser	Outlet temperature, 35°C
Gas Heat Exchanger	Temperature difference: inlet - outlet of stream103, -28°C Temperature difference: inlet - outlet of stream 2, -25°C
Evaporator	Temperature outlet, -5°C
Solution Tank	Temperature, 37°C

Initial Specifications:

State point PT-1:

Pressure	25 bar
Temperature	38.4°C
H_2O mass fraction	0.65
NH_3 mass fraction	0.35
H_2 mass fraction	0
Total mass flow	0.19 kg/h

State point PT-2:

Pressure	25 bar
Temperature	27.5°C
H_2O mass fraction	0.01
NH_3 mass fraction	0.083
H_2 mass fraction	0.907
Total mass flow	0.019 kg/h

3.6.1 Solution heat exchanger

As shown in Figure 3-4, a two-flow heat exchanger HeatX model is used for the solution heat exchanger (SOLHX) connecting the streams (PT1 with SHX-BP) and (BPPH-SHX with SLHX-ABS).

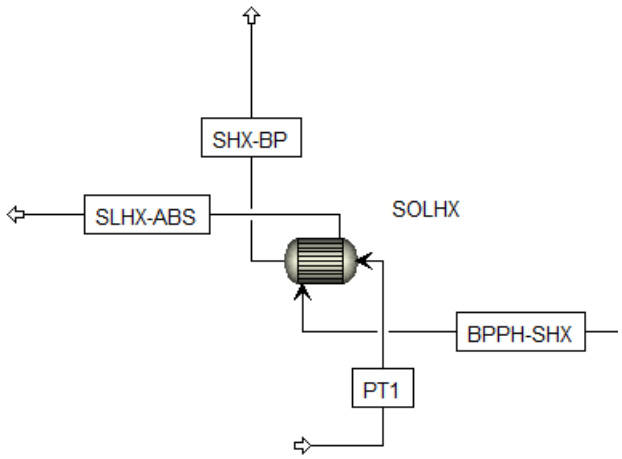

Figure 3-4: Solution heat exchanger model in Aspen Plus

3.6.2 Gas heat exchanger

For the Gas heat exchanger (GHX), a three-flow heat exchanger MHeatX model is used to connect the streams (COND-GHX with GHX-MXE1), (PT2 with GHX-MXE2) and (EVAP-GHX with GHX-ABS) as shown in Figure 3-5. The outlet streams of the GHX are then mixed in the MIX-EVAP and fed to the evaporator.

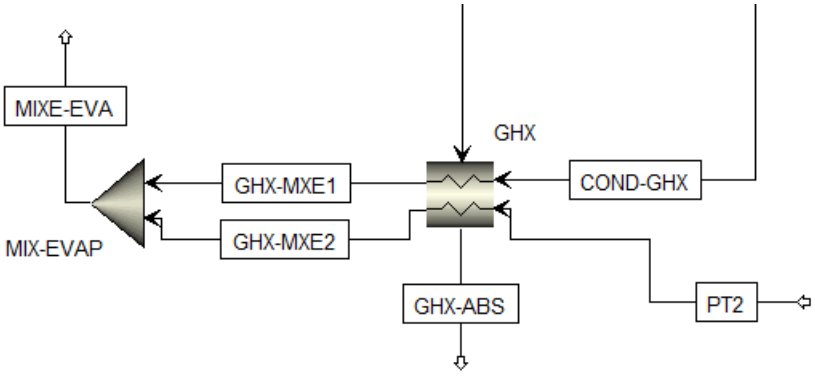

Figure 3-5: Gas heat exchanger Aspen Plus model

3.6.3 Generator

As shown in Figure 3-6, a RadFrac with Reboiled Stripping block is used for the generator (GEN). The streams entering the generator are: BP-GEN-V, BP-GEN-L and REC-GEN. The streams GEN-REC and GEN-BPPR leave the generator at the bottom and the top, respectively.

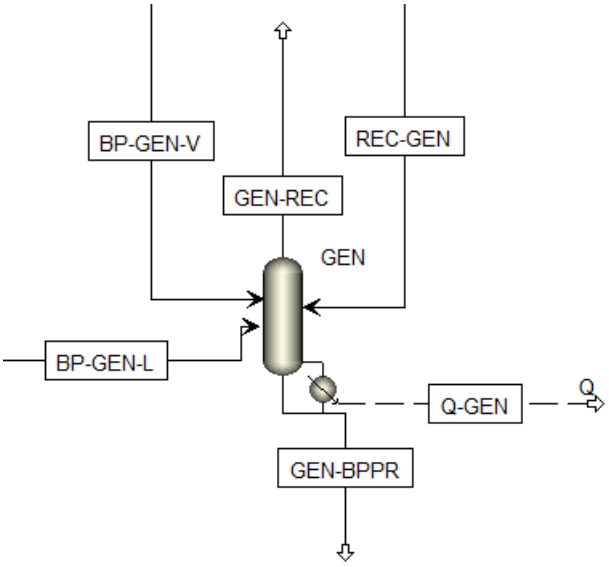

Figure 3-6: Generator Aspen Plus model

3.6.4 Bubble pump

The bubble pump (BBL-PUMP) is modeled by combining a Flash and a Heater block connected with a hot stream (Figure 3-7). SHX-BP represents the stream entering the bubble pump. BP-GEN-V and BP-GEN-L represent the streams leaving the bubble pump streams outlet.

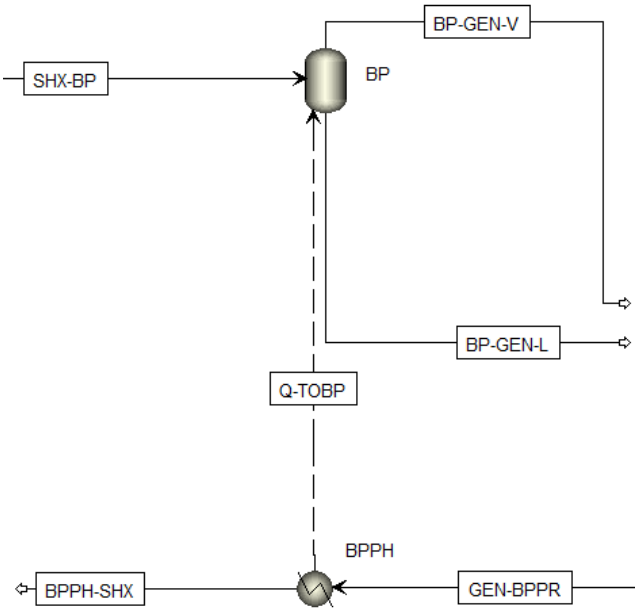

Figure 3-7: Bubble pump Aspen Plus model

3.6.5 Rectifier

The rectifier (RECT) is modeled using a Rectifier block (Figure 3-8). Material stream GEN-REC represents the stream entering the rectifier. Material Streams RECT-CND

and REC-GEN represent the distillate and bottom outlet streams of the rectifier respectively. The heat stream Q-RECT represents the heat loss from the rectifier.

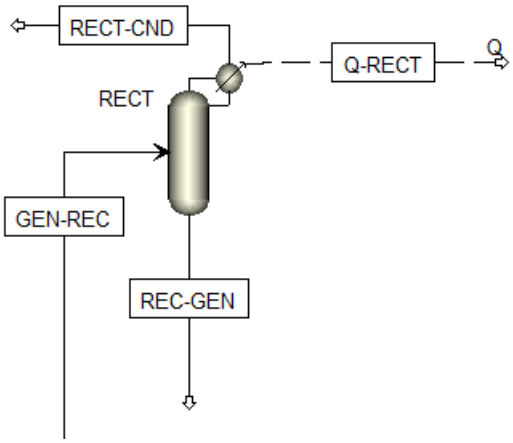

Figure 3-8: Rectifier model in Aspen Plus

3.6.6 Absorber

As shown in Figure 3-9, the absorber (ABSORBER) is modeled using a RadFrac Absorber block. GHX-ABS and SLHX-ABS represent the streams entering the absorber. ABS-MIXG and ABS-STK represent the streams at the absorber outlet. And the heat stream Q-ABS shows the heat loss from the absorber. Absorber efficiency is taken as 90%.

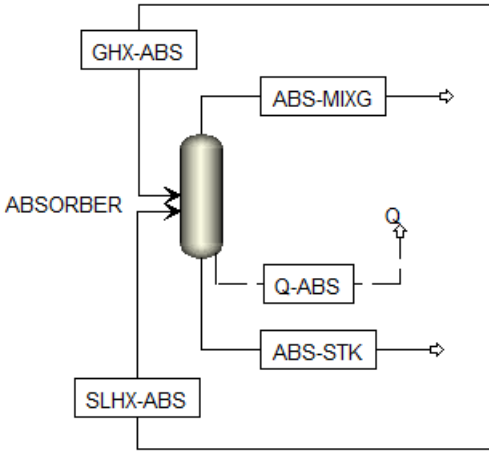

Figure 3-9: Absorber model on Aspen Plus.

3.6.7 Solution Tank

The solution tank (SOLTANK) is modeled using a combination of a Flash and a Mixer (Figure 3-10). ABS-MIXG and ABS-STK represent the inlet streams in the solution

tank. The streams leaving the solution tank are represented by the streams PT1-1 and PT2-2.

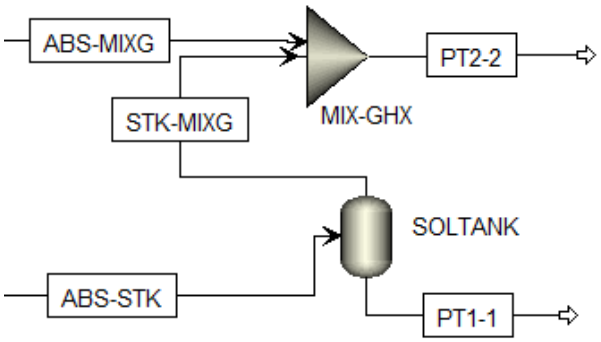

Figure 3-10: Solution tank model in Aspen Plus

3.6.8 Condenser

Regarding the condenser, a Heater block is used between the streams RECT-CND and COND-GHX as shown in Figure 3-11. Q-COND represents the heat ejected from the condenser.

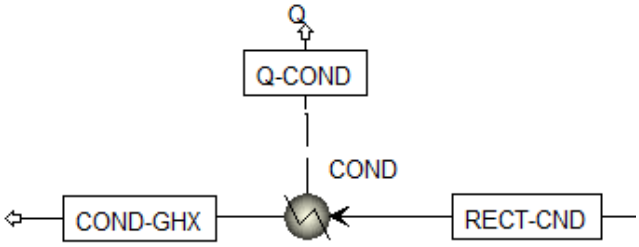

Figure 3-11: Condenser model in Aspen Plus

3.6.9 Evaporator

Similar to the condenser, a Heater block is also used for the evaporator between the streams MIXE-EVA and EVAP-GHX (Figure 3-12). Q-EVAP shows the heat absorbed by the refrigerant due to the evaporation process.

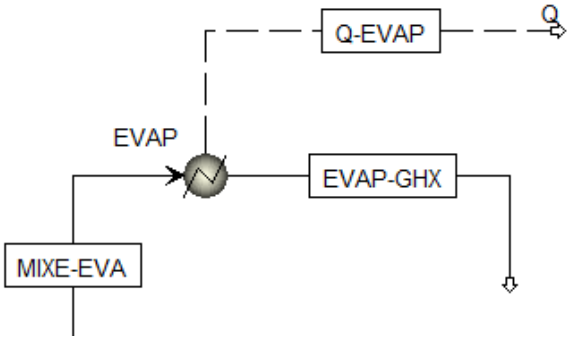

Figure 3-12: Evaporator model in Aspen Plus

3.7 Hourly Solar Insolation Input

In the present study, the system operation will be initially be simulated for a "peak solar" day in Addis Ababa, Ethiopia, using climate data published by Metronorm satellite. The Addis Ababa region experiences high solar irradiance during the summer season, between the months of December to February, with an insolation of 5.2Kwh/m^2. From June onwards, the weather is typically cloudier with periods of heavy rainfall. Insolation data and the solar sun path of Addis Ababa are attached in appendix section.

3.8 Performance Parameter (COP)

The performance of Absorption solar cooling system depends mainly on thermodynamic properties of the working fluid. COP of a DAR system is defined as;

$$COP = \frac{Q_{evap}}{Q_{gen}} \qquad 3.29$$

Where Q_{evap} cooling capacity of the evaporator (W)

Q_{gen} heat input of the generator (W)

3.9 Simulation Procedure

The refrigerator model developed in this chapter uses, in a first step, a sequential modular approach in which each block is calculated separately. Two "Break points" are used in the sequential approach. The first "break" is inserted at PT1 (ammonia-rich solution flowing to the solution heat exchanger), and the second "break" at PT2 (ammonia/hydrogen gas mixture flowing to the gas heat exchanger). The identity of state point PT1 on one side and state points PT2 on the other side represent the same state points PT1-1 and PT2-2, respectively. Therefore, state point PT1-1 should have

the same characteristics as those given as inputs at the inlet of the solution heat exchanger (ammonia-rich solution flowing to the solution heat exchanger) after the simulation is run. Also, state point PT2-2 should have the same characteristics as those given as inputs at the inlet of the gas heat exchanger (ammonia/hydrogen gas mixture flowing to the gas heat exchanger) after the simulation is run. These two "Break points" constitutes the simulation convergence criterion in the sequential approach.

4 RESULT AND DISCUSSION

The modeling results were obtained using methodology explained in previous section. Moreover, they have been validated being compared with previous experimental findings (Mansuri, 2016). In a first step to validate the Aspen-Plus model developed for the diffusion-absorption refrigerator, a reference data for a heating power of 46W are used. The corresponding simulation results are reported in Table 4-1.

The temperature of the bottom distillate from the generator is the maximum temperature achieved in the DAR machine and is called the driving or generating temperature. To satisfy the design evaporator temperature of -5.6^{o}C, the simulation result showed that the generator should run at 191.297^{o}C, which is very close to the reference temperature of 191.3^{o}C. This temperature is determined by the heat supplied by the generator. Whereas the lowest temperature of -23^{o}C is observed at the inlet of the absorber (EIN-EVAP) just after expansion of the refrigerant Ammonia in Hydrogen gas.

From Table 4-1, it can also be observed that the mass fraction of Ammonia, Water and Hydrogen as the fluid enters the evaporator (EIN-EVAP) are 74.4%, 0.28% and 24.3% respectively. The presence of water in this stream is relatively very low. However, if large fraction of water is found in the fluid that is entering the evaporator, the heat absorbed by the evaporation process could reduce significantly. The effect of purity of the refrigerant is discussed later in detail.

Mass fraction of water as it leaves the generator is 5.7%. This value is too high to pass through the condenser and the evaporator. Therefore, a rectifier is used in order to further separate the refrigerant ammonia from the water. After rectification (RECT-CND), the mass fraction of water reduces to insignificant value (7.36E-08). This is a necessary step in order to optimize the sub cooling process of ammonia in the condenser and for efficient absorption of heat in the evaporator.

4.1 Validation

Table 4-3 and Figure 4-1 shows a tabular and graphical comparison of simulated and reference temperatures respectively (Mansouri, R. et al, 2019). As it can be seen from the graph, the simulated and the reference temperatures agree in good manner with variation ranging between 0 to 10.58%. Maximum variation was observed at state point ABS-GHX (stream line from absorber to gas heat exchanger) and at state point PT2-2.

Table 4-2 presents the heats absorbed and released during the process in watts. Heat is released to the surrounding at the absorber, rectifier and condenser while heat is absorbed at the evaporator and condenser. Performing energy balance of these heat streams gives a value of -1.04, which is not zero but is very close. The heat absorbed in the generator is calculated to be -45.97W, while the heat absorbed at the evaporator is -7.49W. The values are compared with reference values in Table 4-4. From the table, it can be seen that the simulated value of Q_{evap} shows slightly higher deviation from the reference value by 1.806%. While the calculated COP of the simulated results is 0.161, which is slightly higher than the COP calculated from reference values with a deviation of only 1.874%. Overall, the simulated results show good agreement with reference values.

While passing through the evaporator, the refrigerant begins to vaporize as it absorbs heat from the cooling space. It is to be noted that the pressure and temperature of the refrigerant increases as it travels through the evaporator. This is a unique characteristic of a DAR system. In other types of refrigeration systems like vapor compression and absorption refrigeration systems, compressor or pump and other devices are used to increase or decrease refrigerant pressure. In DAR systems, this is avoided by using a third fluid, in this case Hydrogen gas. In vapor compression or absorption refrigeration, evaporation process is accomplished at constant pressure and temperature. Whereas, in DAR systems, there is a change in both partial pressure and temperature of the refrigerant as it passes through the evaporator. This is clearly depicted in Figure 4-2.

Table 4-1: Aspen-Plus simulation result of the DAR machine.

State Point	From	To	P (bar)	T (°C)	Vapor Fraction	Total Mass Flow Rate (Kg/hr)	Mass Fraction of Ammonia	Mass Fraction of Water	Mass Fraction of Hydrogen
ABS-GHXI	ABSORBER	GHXIN	25	24.5916	1	0.019	0.0860646	0.00700284	0.906933
ABS-STAN	ABSORBER	SOLTANK	25	35.8	0	0.190	0.349691	0.650302	6.72E-06
BP-GEN	BUBP	GEN	25	128.326	0	0.190	0.35	0.65	0
BPPR-SHX	B18	SOLHX	25	166.997	0	0.141	0.12411	0.87589	0
COND-GHX	COND	GHX	25	35	0	0.049	1	7.36E-08	0
EIN-EVAP	B1	EVAP	25	-23.0443	0.801	0.068	0.743779	0.00279417	0.253426
EVAP-GHX	EVAP	GHX	25	-5.6	0.876	0.068	0.743779	0.00279417	0.253426
GEN-BPPR	GEN	B18	25	191.297	0	0.141	0.12411	0.87589	0
GEN-REC	GEN	RECT	25	123.146	1	0.091	0.943095	0.0569049	0
GHX-ABS	GHX	ABSORBER	25	6.0238	0.964	0.068	0.743779	0.00279417	0.253426
GHX-EIN1	GHX	B1	25	5	0	0.049	1	7.36E-08	0
GHX-EIN2	GHX	B1	25	5.5	0.999	0.019	0.083	0.01	0.907

PT1		***SOLHX***	***25***	***38.4***	***0***	***0.190***	***0.35***	***0.65***	***0***
PT1-1	***SOLTANK***		***25***	***38.4***	***0***	***0.190***	***0.349691***	***0.650303***	***6.40E-06***
PT2		***GHX***	***25***	***27.5***	***0.99995***	***0.019***	***0.083***	***0.01***	***0.907***
PT2-2	***GHXIN***		***25***	***24.5916***	***1***	***0.0190001***	***0.0860676***	***0.0070028***	***0.90693***
REC-GEN	RECT	GEN	25	64.3059	0	0.042	0.876706	0.123294	0
RECT-CND	RECT	COND	25	58.3097	1	0.049	1	7.36E-08	0
S56	SOLTANK	GHXIN	25	38.4	1	1.28E-07	0.526681	0.00614134	0.467178
SHX-BP	SOLHX	BUBP	25	110	0	0.190	0.35	0.65	0
SLHX-ABS	SOLHX	ABSORBER	25	70.066	0	0.141	0.12411	0.87589	0

Table 4-2: Aspen Plus simulated results of heat streams

Parameter	**Q_{ABS}**	**Q_{COND}**	**Q_{EVAP}**	**Q_{GEN}**	**Q_{RECT}**
Simulated result (Watts)	12.67	16.01	-7.40	-45.97	23.65

Table 4-3: Comparison of simulated and reference temperatures at different state points

State Point	T Simulated (ºC)	T Reference (ºC)	Error	Error (%)
ABS-GHXI	24.5916	27.5	0.10576	10.58
ABS-STAN	35.8	35.8	0	0.00
BP-GEN	128.326	128.3	0.000203	0.02
BPPR-SHX	166.997	167	1.8E-05	0.00
COND-GHX	35	35	0	0.00
EIN-EVAP	-23.0443	-23	0.001926	0.19
EVAP-GHX	-5.6	-5.6	0	0.00
GEN-BPPR	191.297	191.3	1.57E-05	0.00
GEN-REC	123.146	122.4	0.006095	0.61
GHX-EIN1	5	5	0	0.00
GHX-EIN2	5.5	5.5	0	0.00
PT1	***38.4***	38.4	0	0.00
PT1-1	***38.4***	38.4	0	0.00
PT2	***27.5***	27.5	0	0.00
PT2-2	***24.5916***	27.5	0.10576	10.58
REC-GEN	64.3059	64.1	0.003212	0.32
RECT-CND	58.3097	62	0.059521	5.95
SHX-BP	110	110	0	0.00
SLHX-ABS	70.066	71.1	0.014543	1.45429

Table 4-4: Comparison of simulated and reference heat stream values

Parameter	Simulated	Reference	Deviation
Q_{GEN}	-45.969	-46.000	-0.067%
Q_{EVAP}	-7.401	-7.270	1.806%
COP	0.161	0.158	1.874%

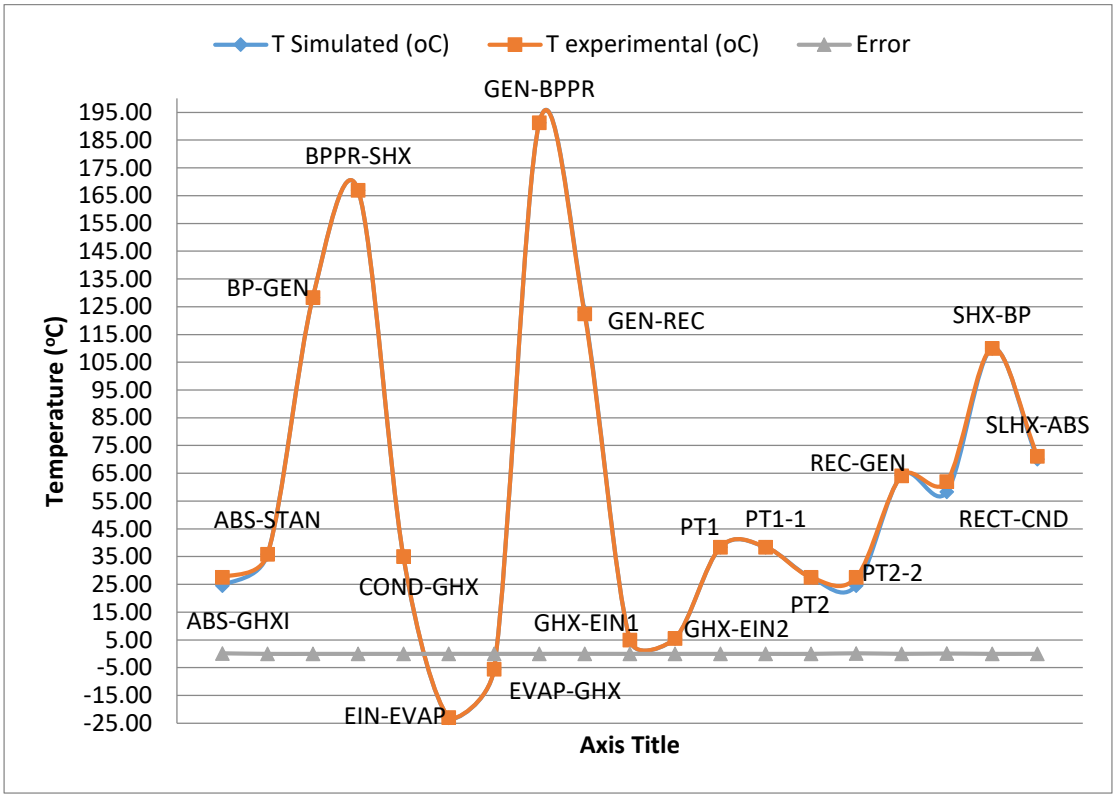

Figure 4-1: Graphical representation of simulated and reference temperatures at state points of the DAR machine

As can be seen from Figure 4-2, at the inlet of the evaporator the partial pressure of the refrigerant is reduced significantly from 25 bars to around 2 bars, since it has been mixed with hydrogen coming from absorber. This enables the evaporation process to start at -23^{o}C in order to end at -5.6^{o}C. However, the partial pressure and temperature of the inert gas H_2 is decreased in a slight manner. This system of reducing partial pressure of the refrigerant at the inlet of the evaporator in DAR machines helps to avoid the use of any mechanical pump or compressor to affect pressure. As the refrigerant absorbs heat energy from the cooling space its partial pressure and temperature increase.

As the refrigerant travels through the evaporator, as can be seen on the figure below, the vapor fraction also increases steadily. This is well expected since the fluid is absorbing heat from the cooling space.

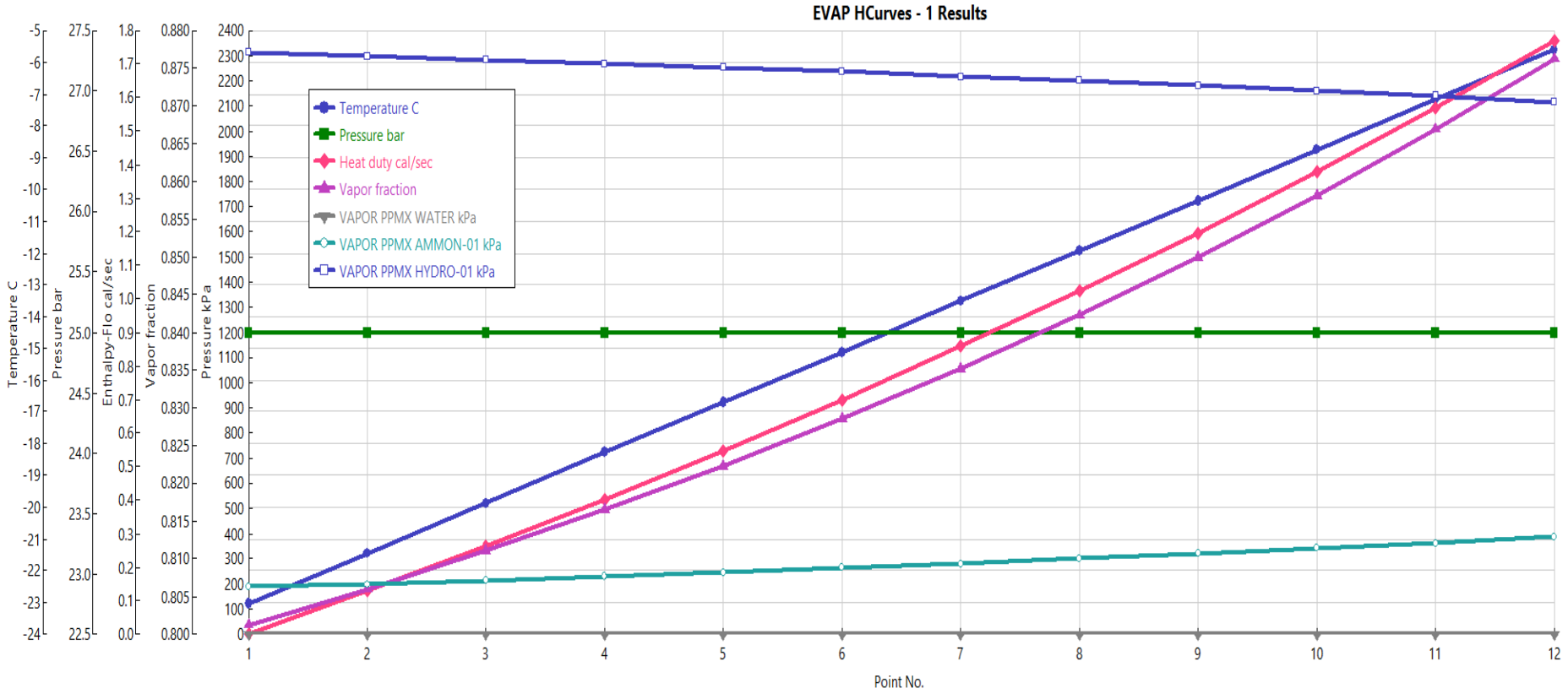

Figure 4-2: Evolution of the partial pressure, vapor fraction, and temperature of the NH_3/H_20 mixture in the evaporator.

4.2 Results

In case of solar driven diffusion absorption refrigeration systems, the generator temperature is highly influenced by the available solar insolation. Figure 4-3 shows the effect of generator heat on the generator temperature in the diffusion absorption cycle with a fixed evaporation temperature of -5.6^{o}C, condensation temperature of 35°C and absorption temperature of 38.5^{o}C for a system pressure of 25 bar. As can be seen from the figure below, as more heat is supplied to the generator, generator temperature (T_{gen}) increases sharply. However, staring from generator heat of 250Watts, increasing generator heat seems to have less effect and temperature increases only slightly.

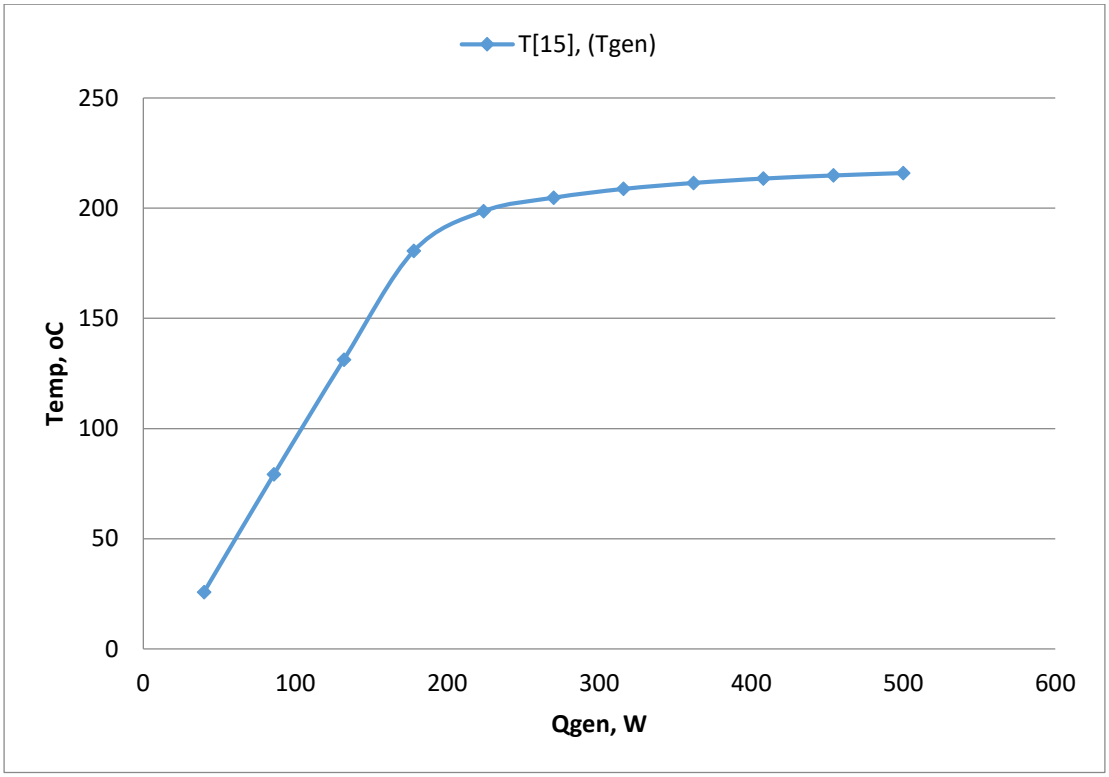

Figure 4-3: Effect of the generator heat on the generator temperature.

One of an important factor in the efficiency of DAR machines is the purity of the refrigerant at the exit of the rectifier. Since it is not practical to achieve 100% purity of refrigerant, it is important that the amount of the absorber, in this case water, to be as small as possible. The effect of refrigerant purity on Qevap, Qabs and Qrect is illustrated in Figure 4.4.

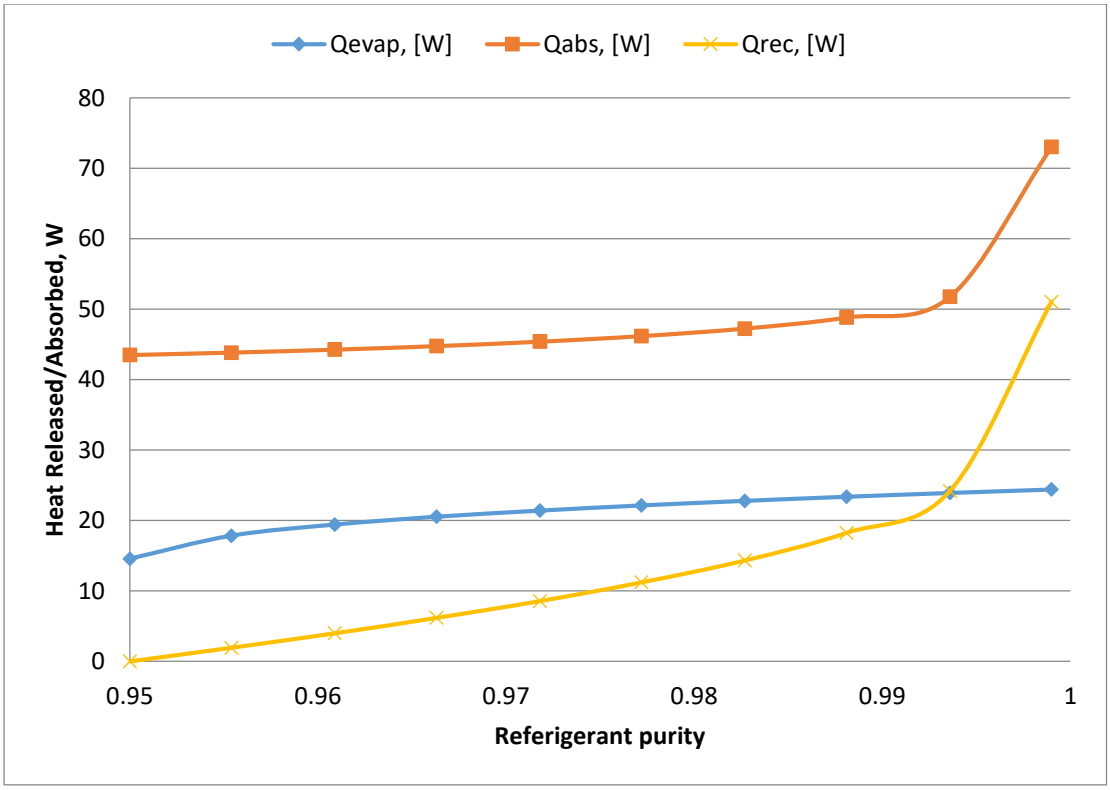

Figure 4-4: Effect of refrigerant purity on Qrec, Qevap and Qabs (at Qgen = 100W)

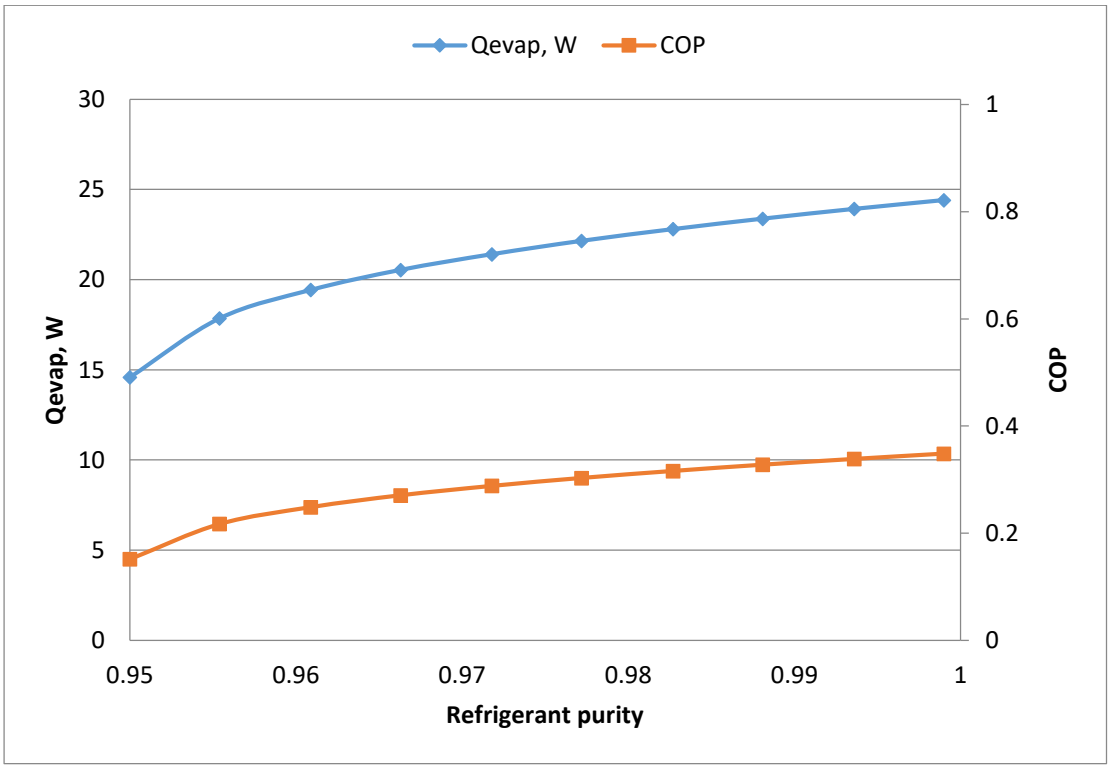

Figure 4-5: Effect of refrigerant purity on Qevap and COP

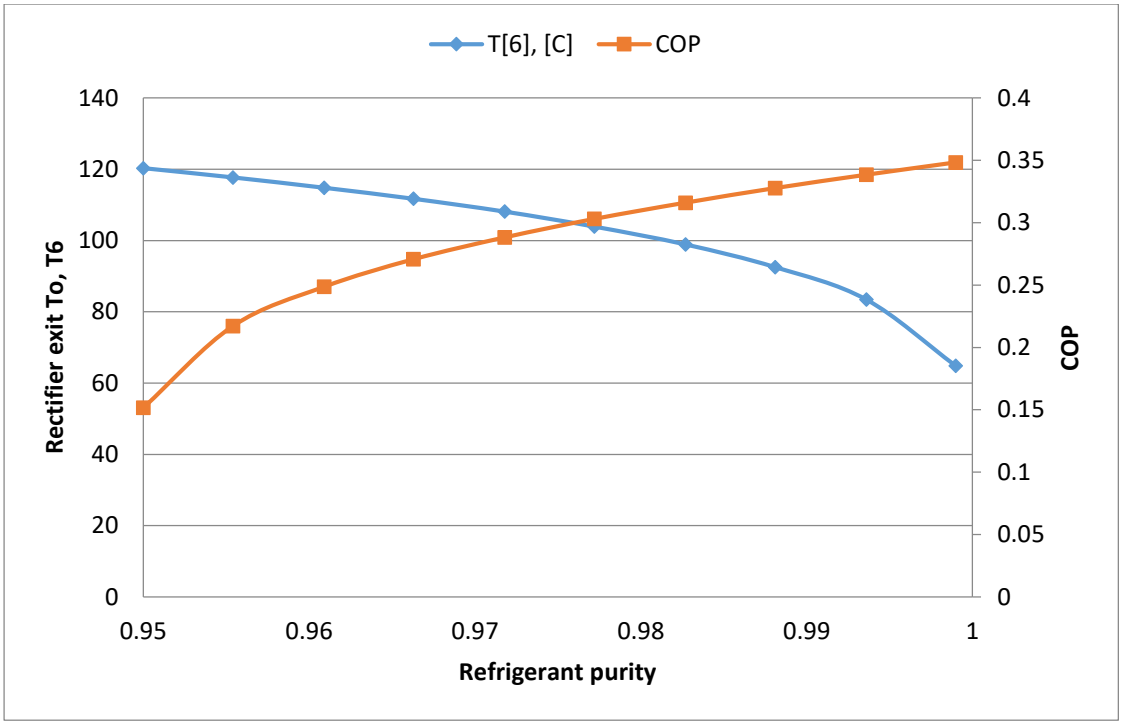

Figure 4-6: Effect of refrigerant purity on rectifier exit temperature and the respective COP

Figure 4-4, 4-5 and 4-6 shows the effect of refrigerant purity at the inlet of the condenser on different parameters. Figure 4-4 describes the heat absorbed by the rectifier generally increases while the heat absorbed by the absorber and the heat rejected by the rectifier show a sharp increase for purity value 0.995. However, the heat absorbed in the evaporator shows slight increment throughout the purity range, starting from 15W to 24W.

This presence of more refrigerant will result in higher amount of ammonia to evaporate and to absorb heat from the cooling space. This will cause the COP of the system to increase from 0.15 to 0.36 as depicted in Figure 4-5.

On the other hand, Figure 4-6 shows the rectifier exit temperature (T_6) and the respective COP for similar range of purity. T_6 decreases from 120^{o}C to 62^{o}C as the purity increases from 0.950 to 0.999. This is because as less water is present in the solution (meaning mass fraction of ammonia is relatively high), the bubble point temperature decreases as can be seen in the following ammonia-water P-T-x diagram.

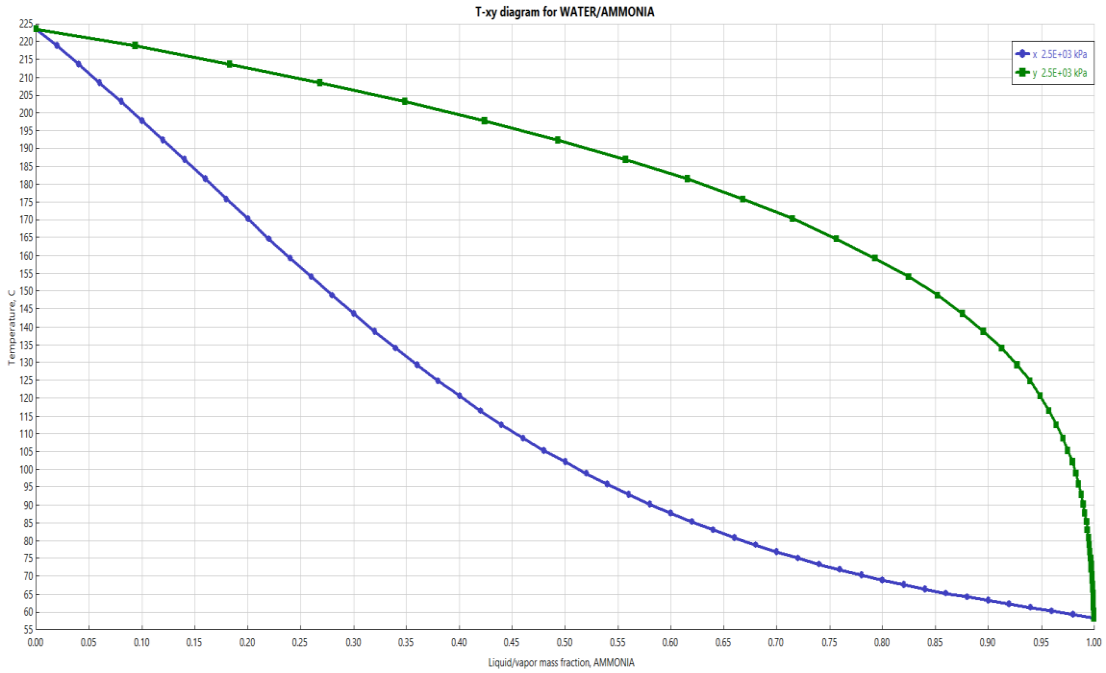

Figure 4-7: P-T-x diagram of NH_3-H_20 solution at 25 bars.

Figure 4-8 below depicts the variation on different heat parameters of each component while varying mass flow rate, at generator heat input of 100W per 1 kg/hr mass flow rate. As the mass flow rate increases from 0.5 kg/hr to 5.5 kg/hr, the heat released or absorbed at the different components, i.e. Qevap, Qabs, Qcond and Qrect increases linearly. The degree of increment for Qevap, Qrect, Qcond and Qabs increase respectively. While Qevap increases with lowest degree, Qabs increases in highest degree of all. It can be understood form this figure that increasing mass flow rate may not have significant effect on heat absorbed by the evaporator. And could lead to a negative effect on the coefficient of performance because of high increase in generator heat while heat absorbed by the evaporator remains low.

The effect of hydrogen mass fraction at the absorber outlet on heat absorbed at the evaporator and COP is shown on Figure 4-9. Both Qevap and COP increase steadily and with similar degree of increments as hydrogen mass fraction increases from 0.5 to 0.95. This can be due to the higher reduction of the partial of the refrigerant at evaporator inlet causing the refrigerant to lower its temperature further. This causes higher amount of heat to be absorbed, and at the same time increasing COP of the system from 0.23 to 0.3 at generator heat of 50W.

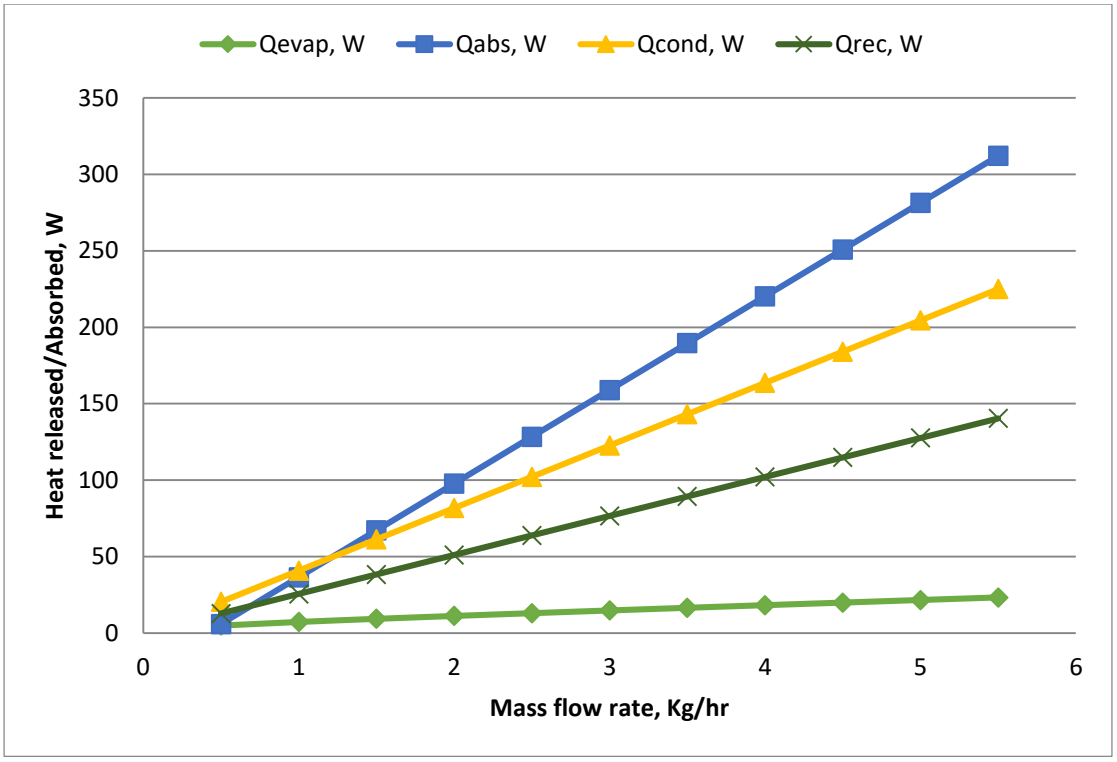

Figure 4-8: Effect of mass flow rate of strong solution on Qevap, Qabs, Qcond and Qrec (at Qgen = 100W/kg)

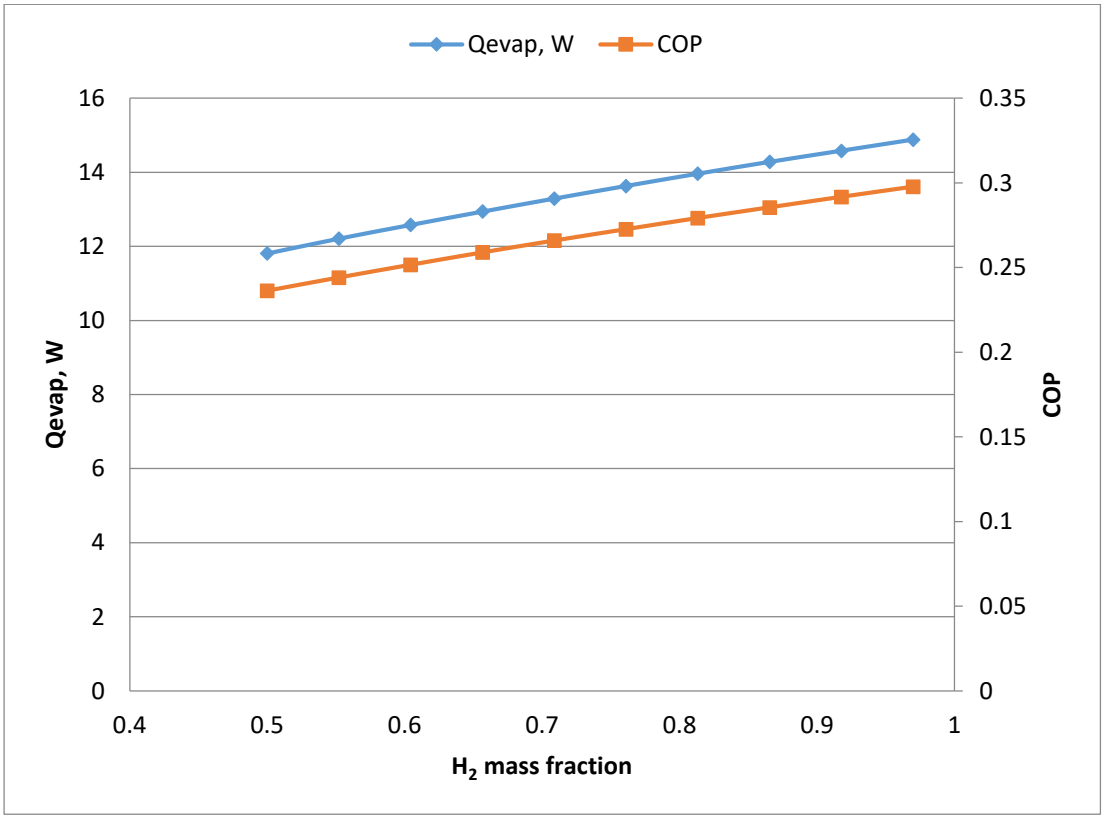

Figure 4-9: Effect of hydrogen mass fraction from the absorber outlet on Qevap and COP (Qgen = 50W)

Figure 4-10 depicts the effects of ammonia mass fraction on coefficient of performance, heat absorbed at the evaporator and heat rejected at the rectifier and condenser. It depicts that coefficient of performance increases almost linearly with an increase in ammonia mass fraction. It can be seen from the figure that the heat released at the condenser increases rapidly to about 27W as ammonia mass fraction increases from 0.05 to 0.4. Similarly, the COP of the system shows significant increase to about 0.28 from 0.05.

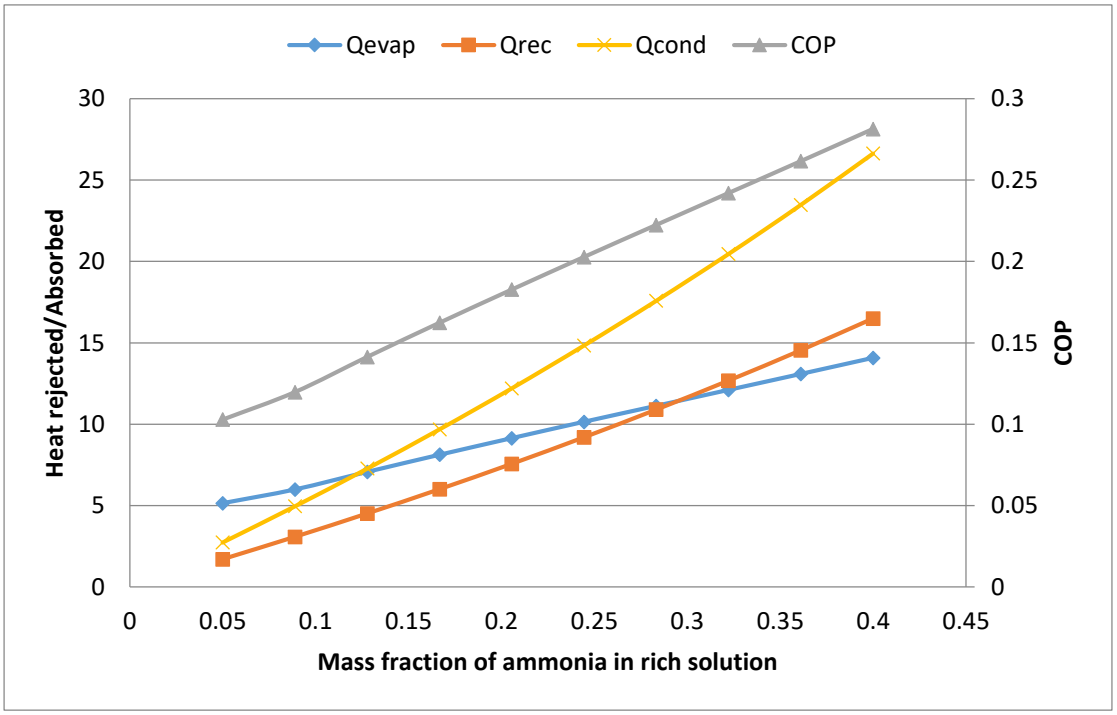

Figure 4-10: Effect of mass fraction of ammonia in rich solution on heat rejected, heat absorbed and COP (at Qgen = 50W)

The increased amount of ammonia concentration will release more amount of refrigerant vapor per unit mass of mixture flow. Moreover, heat added to the low mass fraction of ammonia solution mixture will be removed in rectifier and absorber with little bit contribution to the cooling capacity. This will affect coefficient of performance adversely. So, a minimum amount of ammonia mass fraction in the solution is required to start diffusion absorption refrigeration cycle normally. On contrary for higher concentrations it becomes more difficult for ammonia vapor to be reabsorbed in the absorber for the specified pressure. From the literature study, it was found that a minimum concentration, say 30%, should be needed to run the system without detrimental effects, thus increasing COP and cooling effect for low heat supplied to the generator or lower availability of solar radiations.

5 CONCLUSION AND RECOMMENDATION

For a modest capacity diffusion-absorption refrigerator, an Aspen-Plus steady-state model was created. A set of assumptions derived from earlier literature reviews were added as inputs for the simulations. The computed findings for the 46 Watt heating rates were fairly close to the reference temperature values. There were only 11% or less differences between the expected and measured values. This suggests that the model created accurately represents the operation of the bubble pump absorption refrigerator. This simulation based on thermodynamic modeling has been carried out in the present work to predict the performance of the diffusion absorption refrigeration cycle for concentration of the tertiary fluid, which is hydrogen in this case and other key parameters like refrigerant purity, generator heat and concentrations of the refrigerant in the rich solution. It is concluded that in general, the performance of diffusion absorption refrigeration cycle operating with NH_3-H_2O-H_2 can be a viable commercial product with more additional researches done. Improvements in lowering the amount of heat lost during cooling process in the rectifier, condenser and absorber can significantly improve the performance. Bubble pump refrigeration holds many advantages as it is free from moving parts and requires very small maintenance. The additional advantage of this system is that the system can utilize heat sources like solar, geothermal, and industrial waste or others in place of conventional energy sources. Furthermore, incorporation of hot storage system for the machine to work at night can be studied for future works. In addition, better performing fluid mixtures should be explored in order to improve the performance of the system.

REFERENCES

Acuña, A., Lara, F., Velázquez, N., & Cerezo, J. (2014). Optimum generator temperature to couple different diffusion absorption solar cooling systems. *Energy Economics*, *45*(June), 128–135. https://doi.org/10.1016/j.ijrefrig.2014.05.016

Adjibade, M. I. S., Thiam, A., Awanto, C., Ndiogou, B. A., & Sambou, V. (2017). Dynamic investigation of the diffusion absorption refrigeration system NH3-H2O-H2. *Case Studies in Thermal Engineering*, *10*(October), 468–474. https://doi.org/10.1016/j.csite.2017.10.006

Al-Alili, A., Islam, M. D., Kubo, I., Hwang, Y., & Radermacher, R. (2012). Modeling of a solar powered absorption cycle for Abu Dhabi. *Applied Energy*, *93*, 160–167. https://doi.org/10.1016/j.apenergy.2010.11.034

Alazazmeh, A. J., & Mokheimer, E. M. (2015). Review of Solar Cooling Technologies. *Journal of Applied Mechanical Engineering*, *04*(05). https://doi.org/10.4172/2168-9873.1000180

Analysis, T., Solar, O. F., Absorption, P., For, S., Of, C., & Fluids, W. (1987). *I . Ziegler Band Trepp Ch : Equation of State for Ammonia / Water Mixtures . Int .* 49–50.

Baldwin, C., & Cruickshank, C. A. (2012). A review of solar cooling technologies for residential applications in Canada. *Energy Procedia*, *30*, 495–504. https://doi.org/10.1016/j.egypro.2012.11.059

Ben Ezzine, N., Garma, R., & Bellagi, A. (2010). A numerical investigation of a diffusion-absorption refrigeration cycle based on R124-DMAC mixture for solar cooling. *Energy*, *35*(5), 1874–1883. https://doi.org/10.1016/j.energy.2009.12.032

Ben Jemaa, R., Mansouri, R., & Bellagi, A. (2016). Dynamic testing and modeling of a diffusion absorption refrigeration system. *International Journal of Refrigeration*, *67*, 249–258. https://doi.org/10.1016/j.ijrefrig.2016.03.008

Benhmidene, A., Chaouachi, B., Bourouis, M., & Gabsi, S. (2011). Effect of operating conditions on the performance of the bubble pump of absorption-

diffusion refrigeration cycles. *Thermal Science*, *15*(3), 793–806. https://doi.org/10.2298/TSCI100601002B

Benhmidene, A., Hidouri, K., & Chaouachi, B. (2017). *Investigation of Pumping Action of Bubble Pump of Diffusion-*. *17*(4).

Chauhan, P. R., Kaushik, S. C., & Tyagi, S. K. (2022). Current status and technological advancements in adsorption refrigeration systems: A review. *Renewable and Sustainable Energy Reviews*, *154*, 111808. https://doi.org/10.1016/J.RSER.2021.111808

Dardouch, J., Charia, M., Bernatchou, A., Dardouch, A., Malaine, S., & Jeffali, F. (2019). Study of a solar absorption refrigeration machine in the Moroccan climate. *Materials Today: Proceedings*, *13*, 1197–1204. https://doi.org/10.1016/j.matpr.2019.04.088

Dutil, Y. and, & Rousse, D. (2010). A Review of Active Solar Cooling Technologies. *Industrial Research Chair in Technologies of Energy and Energy Efficiency*, *January 2010*, 9. http://www.t3e.info/pdf/Publications/2010_PALENC_Solar_cooling.pdf

Engineering, M., Manahil, B., Sc, W. A. B., & Sc, K. M. (1999). *Design and Construction of a Continuous Solar Absorption Refrigeration Unit*. *1993*.

Freeman, J., Najjaran, A., Edwards, R., Reid, M., Hall, R., Ramos, A., & Markides, C. N. (2017). Testing and simulation of a solar diffusion-absorption refrigeration system for low-cost solar cooling in India. *ISES Solar World Congress 2017 - IEA SHC International Conference on Solar Heating and Cooling for Buildings and Industry 2017, Proceedings*, 1711–1722. https://doi.org/10.18086/swc.2017.28.07

Harraz, A. A., Freeman, J., Wang, K., Dowell, N. Mac, & Markides, C. N. (2019). Diffusion-absorption refrigeration cycle simulations in gPROMS using SAFT-γ Mie. *Energy Procedia*, *158*, 2360–2365. https://doi.org/10.1016/j.egypro.2019.01.284

He, T., & Lin, W. (2020). Design and optimization of integrated single mixed refrigerant processes for coproduction of LNG and high-purity ethane.

International Journal of Refrigeration, *119*, 216–226. https://doi.org/10.1016/J.IJREFRIG.2020.06.033

Ileri, A. (1995). Yearly simulation of a solar-aided R22-DEGDME absorption heat pump system. *Solar Energy*, *55*(4), 255–265. https://doi.org/10.1016/0038-092X(95)00043-Q

Jelinek, M., Levy, A., & Borde, I. (2016). The influence of the evaporator inlet conditions on the performance of a diffusion absorption refrigeration cycle. *Applied Thermal Engineering*, *99*, 979–987. https://doi.org/10.1016/j.applthermaleng.2016.01.152

Mansouri, R., Bourouis, D. M., & Dr. Ahmed Bellagi. (1996). *ABSORPTION / DIFFUSION REFRIGERATING MACHINES USING AMMONIA AS A REFRIGERANT : SIMULATION UNDER STEADY-STATE AND DYNAMIC REGIMES The eoretic cal and d expe riment tal stud dy of a absorpt tion an nd abs orption n / diffus sion re efrigera ating m machin e*. 35.

Mbarek, R., & Mbarek, W. (2013). Building and Experimentation of Diffusion Absorption Refrigeration Machines. *International Journal of Basics and Applied Sciences*, *1*(3), 605–612. http://insikapub.com/Vol-01/No-03/16IJBAS(1)(3).pdf

Mittal, V., Kasana, K. S., & Thakur, N. S. (2006). Modelling and simulation of a solar absorption cooling system for India. *Journal of Energy in Southern Africa*, *17*(3), 65–70. https://doi.org/10.17159/2413-3051/2006/v17i3a3290

Najjaran, A., Harraz, A. A., Freeman, J., Dowell, N. Mac, & Markides, C. N. (2018). Numerical and experimental investigation of diffusion absorption refrigeration systems for use with low-temperature heat sources. *ECOS 2018 - Proceedings of the 31st International Conference on Efficiency, Cost, Optimization, Simulation and Environmental Impact of Energy Systems*.

Noor, D. N., Arshad, A., Azran, Z., Ibrahim, H., & Basrawi, F. (2016). A review on the recent development of solar absorption and vapour compression based hybrid air conditioning with low temperature storage. *MATEC Web of Conferences*, *38*. https://doi.org/10.1051/matecconf/20163802007

Ojha, M. K., Shukla, A. K., Verma, P., & Kannojiya, R. (2020). Recent progress and

outlook of solar adsorption refrigeration systems. *Materials Today: Proceedings*. https://doi.org/10.1016/j.matpr.2020.09.593

Özbaş, E. (2018). Experimental Study Of Diffusion Absorption Refrigeration Systems Using Solar Energy. *Journal of Polytechnic*, *0900*(2), 291–297. https://doi.org/10.2339/politeknik.385931

Rabeb, J., Ali, B., Khaoula, H., & Bechir, C. (2017). *Simulation of Ammonia-Water Two Phase Flow in Bubble Pump*. *11*(8), 1473–1477.

Rodríguez-Muñoz, J. L., & Belman-Flores, J. M. (2014). Review of diffusion-absorption refrigeration technologies. In *Renewable and Sustainable Energy Reviews* (Vol. 30, pp. 145–153). Pergamon. https://doi.org/10.1016/j.rser.2013.09.019

Shankar Ganesh, N., & Srinivas, T. (2011). Evaluation of thermodynamic properties of ammonia- water mixture up to 100 bar for power application systems. *Journal of Mechanical Engineering Research*, *3*(1), 25–39. http://www.academicjournals.org/jmer

Shihab, A. S., & Faisal, S. H. (2015). An Approach for Modeling the Performance. *Iraqi, The For, Journal Engineering, Material*, *15*, 49–65.

Taieb, A., Mejbri, K., & Bellagi, A. (2016). Detailed thermodynamic analysis of a diffusion-absorption refrigeration cycle. *Energy*, *115*, 418–434. https://doi.org/10.1016/j.energy.2016.09.002

Ting, D. S., & Aman, J. (2016). *Modelling and Analysis of Bubble Pump Parameters for Vapor Absorption Refrigeration Systems Modelling and Analysis of Bubble Pump Parameters for Vapor Absorption Refrigeration Systems*. *June*.

Tozer, R., & James, R. W. (1998). Heat powered refrigeration cycles. *Applied Thermal Engineering*, *18*(9–10), 731–743. https://doi.org/10.1016/s1359-4311(97)00112-9

Wang, H. (2012). A new style solar-driven diffusion absorption refrigerator and its operating characteristics. *Energy Procedia*, *18*, 681–692. https://doi.org/10.1016/j.egypro.2012.05.083

Zulu, A. (2000). *Thermodynamic Analysis of a Three-Fluid Absorption Refrigeration*

Machine. University of Cape Town.

APPENDIX A1: ASPEN PLUS SIMULATION RESULT

		Material									
Stream Name	**Units**	**ABS-GHXI**	**ABS-STAN**	**BP-GEN**	**BPPR-SHX**	**COND-GHX**	**EIN-EVAP**	**EVAP-GHX**	**GEN-BPPR**	**GEN-REC**	**GHX-ABS**
Description											
From		ABSORBER	ABSORBER	BUBP	B18	COND	B1	EVAP	GEN	GEN	GHX
To		GHXIN	SOLTANK	GEN	SOLHX	GHX	EVAP	GHX	B18	RECT	ABSORBER
Stream Class		CONVEN	CONVEN	CONVEN	CONVEN	CONVEN	CONVEN	CONVEN	CONVEN	CONVEN	CONVEN
Phase		Vapor Phase	Liquid Phase	Liquid Phase	Liquid Phase	Liquid Phase			Liquid Phase	Vapor Phase	
Temperature	C	24.5916	35.8	128.326	166.997	35	-23.0443	-5.6	191.297	123.146	6.0238
Pressure	bar	25	25	25	25	25	25	25	25	25	25
Molar Vapor Fraction		1	0	0	0	0	0.801162	0.876219	0	1	0.964422
Molar Liquid Fraction		0	1	1	1	1	0.198838	0.123781	1	0	0.035578
Molar Solid Fraction		0	0	0	0	0	0	0	0	0	0
Mass Vapor Fraction		1	0	0	0	0	0.426342	0.642953	0	1	0.897265
Mass Liquid Fraction		0	1	1	1	1	0.573658	0.357047	1	2.72E-07	0.102735
Mass Solid Fraction		0	0	0	0	0	0	0	0	0	0
Molar Enthalpy	cal/mol	-176.28	-50022.8	-48136.6	-59297.6	-15801.3	-4346.31	-3793.94	-58771.9	-12876.7	-3248.31
Mass Enthalpy	cal/gm	-80.2668	-2832.98	-2726.06	-3315.14	-927.819	-736.888	-643.238	-3285.75	-753.741	-550.729
Molar Entropy	cal/mol-K	-6.53511	-41.1478	-35.8585	-32.7687	-44.2813	-16.6956	-14.5664	-31.6064	-26.8139	-12.5719
Mass Entropy	cal/gm-K	-2.97567	-2.33035	-2.03073	-1.83199	-2.60011	-2.83063	-2.46964	-1.76701	-1.56956	-2.13148
Molar Density	mol/cc	0.001002	0.042136	0.03785	0.03934	0.030664	0.001489	0.001288	0.037813	0.000848	0.001136
Mass Density	gm/cc	0.002201	0.74401	0.668359	0.703666	0.522217	0.008781	0.007597	0.676358	0.014479	0.006699

Enthalpy Flow	cal/sec	-0.42363	-149.518	-143.876	-129.843	-12.6286	-13.919	-12.15	-128.692	-19.0529	-10.4027
Average MW		2.19618	17.6573	17.6579	17.8869	17.0306	5.8982	5.8982	17.8869	17.0837	5.8982
Mole Flows	kmol/hr	0.008651	0.01076	0.01076	0.007883	0.002877	0.011529	0.011529	0.007883	0.005327	0.011529
WATER	kmol/hr	7.39E-06	0.006858	0.006855	0.006855	2.00E-10	1.05E-05	1.05E-05	0.006855	0.000287	1.05E-05
AMMON-01	kmol/hr	9.60E-05	0.003901	0.003905	0.001028	0.002877	0.00297	0.00297	0.001028	0.005039	0.00297
HYDRO-01	kmol/hr	0.008548	6.33E-07	0	0	0	0.008549	0.008549	0	0	0.008549
Mole Fractions											
WATER		0.000854	0.637381	0.637107	0.869649	6.96E-08	0.000915	0.000915	0.869649	0.053962	0.000915
AMMON-01		0.011099	0.362561	0.362893	0.130351	1	0.257593	0.257593	0.130351	0.946038	0.257593
HYDRO-01		0.988048	5.88E-05	0	0	0	0.741492	0.741492	0	0	0.741492
Mass Flows	kg/hr	0.019	0.19	0.19	0.141	0.049	0.068	0.068	0.141	0.091	0.068
WATER	kg/hr	0.000133	0.123557	0.1235	0.1235	3.61E-09	0.00019	0.00019	0.1235	0.005178	0.00019
AMMON-01	kg/hr	0.001635	0.066441	0.0665	0.0175	0.049	0.050577	0.050577	0.0175	0.085822	0.050577
HYDRO-01	kg/hr	0.017232	1.28E-06	0	0	0	0.017233	0.017233	0	0	0.017233
Mass Fractions											
WATER		0.007003	0.650302	0.65	0.87589	7.36E-08	0.002794	0.002794	0.87589	0.056905	0.002794
AMMON-01		0.086065	0.349691	0.35	0.12411	1	0.743779	0.743779	0.12411	0.943095	0.743779
HYDRO-01		0.906933	6.72E-06	0	0	0	0.253426	0.253426	0	0	0.253426
Volume Flow	l/min	0.143871	0.004256	0.004738	0.00334	0.001564	0.129061	0.149175	0.003474	0.104748	0.169169
Vapor Phase											
Molar Enthalpy	cal/mol	-176.28					-1167.98	-1931.47		-12876.6	-2712.6
Mass Enthalpy	cal/gm	-80.2668					-372.115	-446.275		-753.738	-494.325
Molar Entropy	cal/mol-K	-6.53511					-8.88082	-9.99909		-26.8139	-11.3396
Mass Entropy	cal/gm-K	-2.97567					-2.82941	-2.31033		-1.56956	-2.06645
Molar Density	mol/cc	0.001002					0.001203	0.001134		0.000848	0.001097

Mass Density	gm/cc	0.002201				0.003776	0.004908		0.014479	0.006018
Enthalpy Flow	cal/sec	-0.42363				-2.99669	-5.41985		-19.0528	-8.37799
Average MW		2.19618				3.13875	4.32798		17.0837	5.48748
Mole Flows	kmol/hr	0.008651				0.009237	0.010102		0.005327	0.011119
WATER	kmol/hr	7.39E-06				1.83E-10	2.11E-09		0.000287	2.46E-08
AMMON-01	kmol/hr	9.60E-05				0.000691	0.001556		0.005039	0.002571
HYDRO-01	kmol/hr	0.008548				0.008546	0.008546		0	0.008548
Mole Fractions										
WATER		0.000854				1.99E-08	2.09E-07		0.053962	2.21E-06
AMMON-01		0.011099				0.074785	0.153989		0.946038	0.231211
HYDRO-01		0.988048				0.925215	0.846011		0	0.768787
Mass Flows	kg/hr	0.019				0.028991	0.043721		0.091	0.061014
WATER	kg/hr	0.000133				3.31E-09	3.80E-08		0.005178	4.44E-07
AMMON-01	kg/hr	0.001635				0.011764	0.026492		0.085822	0.043782
HYDRO-01	kg/hr	0.017232				0.017227	0.017228		0	0.017232
Mass Fractions										
WATER		0.007003				1.14E-07	8.69E-07		0.056905	7.27E-06
AMMON-01		0.086065				0.405776	0.605946		0.943095	0.717571
HYDRO-01		0.906933				0.594224	0.394053		0	0.282422
Liquid Phase										
Molar Enthalpy	cal/mol		-50022.8	-48136.6	-59297.6	-15801.3	-17152.5	-16978	-58771.9	-17769.9
Mass Enthalpy	cal/gm		-2832.98	-2726.06	-3315.14	-927.819	-1007.99	-997.919	-3285.75	-1043.34
Molar Entropy	cal/mol-K		-41.1478	-35.8585	-32.7687	-44.2813	-48.183	-46.8978	-31.6064	-45.9766
Mass Entropy	cal/gm-K		-2.33035	-2.03073	-1.83199	-2.60011	-2.83154	-2.75652	-1.76701	-2.69947
Molar Density	mol/cc		0.042136	0.03785	0.03934	0.030664	0.035038	0.034006	0.037813	0.033652
Mass Density	gm/cc		0.74401	0.668359	0.703666	0.522217	0.596231	0.57855	0.676358	0.573153

Enthalpy Flow	cal/sec	-149.518	-143.876	-129.843	-12.6286	-10.9223	-6.7302	-128.692	-2.02466
Average MW		17.6573	17.6579	17.8869	17.0306	17.0166	17.0134	17.8869	17.0317
Mole Flows	kmol/hr	0.01076	0.01076	0.007883	0.002877	0.002292	0.001427	0.007883	0.00041
WATER	kmol/hr	0.006858	0.006855	0.006855	2.00E-10	1.05E-05	1.05E-05	0.006855	1.05E-05
AMMON-01	kmol/hr	0.003901	0.003905	0.001028	0.002877	0.002279	0.001414	0.001028	0.000399
HYDRO-01	kmol/hr	6.33E-07	0	0	0	2.83E-06	2.32E-06	0	6.59E-07
Mole Fractions									
WATER		0.637381	0.637107	0.869649	6.96E-08	0.004601	0.007389	0.869649	0.025653
AMMON-01		0.362561	0.362893	0.130351	1	0.994166	0.990986	0.130351	0.97274
HYDRO-01		5.88E-05	0	0	0	0.001234	0.001625	0	0.001607
Mass Flows	kg/hr	0.19	0.19	0.141	0.049	0.039009	0.024279	0.141	0.006986
WATER	kg/hr	0.123557	0.1235	0.1235	3.61E-09	0.00019	0.00019	0.1235	0.00019
AMMON-01	kg/hr	0.066441	0.0665	0.0175	0.049	0.038813	0.024085	0.0175	0.006795
HYDRO-01	kg/hr	1.28E-06	0	0	0	5.70E-06	4.68E-06	0	1.33E-06
Mass Fractions									
WATER		0.650302	0.65	0.87589	7.36E-08	0.004871	0.007824	0.87589	0.027134
AMMON-01		0.349691	0.35	0.12411	1	0.994983	0.991983	0.12411	0.972675
HYDRO-01		6.72E-06	0	0	0	0.000146	0.000193	0	0.00019

APPENDIX A2: ASPEN PLUS SIMULATION RESULT

Material												
Stream Name	**Units**	**GHX-EIN1**	**GHX-EIN2**	**PT1**	**PT1-1**	**PT2**	**PT2-2**	**REC-GEN**	**RECT-CND**	**S56**	**SHX-BP**	**SLHX-ABS**
Description												
From		GHX	GHX		SOLTANK		GHXIN	RECT	RECT	SOLTANK	SOLHX	SOLHX
To		B1	B1	SOLHX		GHX		GEN	COND	GHXIN	BUBP	ABSORBER
Stream Class		CONVEN	CONVEN	CONVEN	CONVEN	CONVEN	CONVEN	CONVEN	CONVEN	CONVEN	CONVEN	CONVEN
Phase		Liquid Phase		Liquid Phase	Liquid Phase		Vapor Phase	Liquid Phase	Vapor Phase	Vapor Phase	Liquid Phase	Liquid Phase
Temperature	C	5	5.5	38.4	38.4	27.5	24.5916	64.3059	58.3097	38.4	110	70.066
Pressure	bar	25	25	25	25	25	25	25	25	25	25	25
Molar Vapor Fraction		0	0.998764	0	0	0.999952	1	0	1	1	0	0
Molar Liquid Fraction		1	0.001236	1	1	4.81E-05	0	1	0	0	1	1
Molar Solid Fraction		0	0	0	0	0	0	0	0	0	0	0
Mass Vapor Fraction		0	0.989975	0	0	0.999608	1	0	1	1	0	0
Mass Liquid Fraction		1	0.010025	1	1	0.000392	0	1	0	0	1	1
Mass Solid Fraction		0	0	0	0	0	0	0	0	0	0	0
Molar Enthalpy	cal/mol	-16399.5	-337.969	-49959	-49972	-173.37	-176.285	-21683.3	-11012.1	-1283.76	-48521.8	-61259.4
Mass Enthalpy	cal/gm	-962.946	-153.896	-2829.27	-2830.1	-78.945	-80.2686	-1264.62	-646.607	-337.649	-2747.87	-3424.82
Molar Entropy	cal/mol-K	-46.3223	-7.03066	-40.9886	-40.9838	-6.46241	-6.53511	-41.8543	-29.7763	-8.15554	-36.8402	-37.7974
Mass Entropy	cal/gm-K	-2.71995	-3.20145	-2.32126	-2.32106	-2.9427	-2.97567	-2.44104	-1.7484	-2.14503	-2.08633	-2.11313
Molar Density	mol/cc	0.033104	0.001072	0.042035	0.042039	0.000993	0.001002	0.031595	0.001099	0.000965	0.038855	0.0439077
Mass Density	gm/cc	0.563778	0.002355	0.742244	0.74229	0.00218	0.002201	0.541722	0.018724	0.003669	0.6861	0.785374
Enthalpy Flow	cal/sec	-13.1068	-0.81223	-149.322	-149.366	-0.41665	-0.42364	-14.7539	-8.80103	-1.20E-05	-145.027	-134.139

Average MW		17.0306	2.19608	17.6579	17.6574	2.19608	2.19618	17.1461	17.0306	3.80206	17.6579	17.8869
Mole Flows	kmol/hr	0.002877	0.008652	0.01076	0.01076	0.008652	0.008651	0.00245	0.002877	3.36E-08	0.01076	0.00788285
WATER	kmol/hr	2.00E-10	1.05E-05	0.006855	0.006858	1.05E-05	7.39E-06	0.000287	2.00E-10	4.36E-11	0.006855	0.00685532
AMMON-01	kmol/hr	0.002877	9.26E-05	0.003905	0.003901	9.26E-05	9.60E-05	0.002162	0.002877	3.95E-09	0.003905	0.00102754
HYDRO-01	kmol/hr	0	0.008549	0	6.03E-07	0.008549	0.008548	0	0	2.96E-08	0	0
Mole Fractions												
WATER		6.96E-08	0.001219	0.637107	0.637383	0.001219	0.000854	0.117345	6.96E-08	0.001296	0.637107	0.869649
AMMON-01		1	0.010703	0.362893	0.362561	0.010703	0.011099	0.882655	1	0.117581	0.362893	0.130351
HYDRO-01		0	0.988078	0	5.61E-05	0.988078	0.988047	0	0	0.881123	0	0
Mass Flows	kg/hr	0.049	0.019	0.19	0.19	0.019	0.019	0.042	0.049	1.28E-07	0.19	0.141
WATER	kg/hr	3.61E-09	0.00019	0.1235	0.123557	0.00019	0.000133	0.005178	3.61E-09	7.85E-10	0.1235	0.1235
AMMON-01	kg/hr	0.049	0.001577	0.0665	0.066441	0.001577	0.001635	0.036822	0.049	6.73E-08	0.0665	0.0174996
HYDRO-01	kg/hr	0	0.017233	0	1.22E-06	0.017233	0.017232	0	0	5.97E-08	0	0
Mass Fractions												
WATER		7.36E-08	0.01	0.65	0.650303	0.01	0.007003	0.123294	7.36E-08	0.006141	0.65	0.87589
AMMON-01		1	0.083	0.35	0.349691	0.083	0.086068	0.876706	1	0.526681	0.35	0.12411
HYDRO-01		0	0.907	0	6.40E-06	0.907	0.90693	0	0	0.467178	0	0
Volume Flow	l/min	0.001449	0.134467	0.004266	0.004266	0.14528	0.143872	0.001292	0.043616	5.81E-07	0.004615	0.00299221
Vapor Phase												
Molar Enthalpy	cal/mol		-265.497			-170.363	-176.285		-11012.1	-1283.76		
Mass Enthalpy	cal/gm		-121.969			-77.6026	-80.2686		-646.607	-337.649		
Molar Entropy	cal/mol-K		-6.98707			-6.46078	-6.53511		-29.7763	-8.15554		
Mass Entropy	cal/gm-K		-3.20985			-2.94297	-2.97567		-1.7484	-2.14503		
Molar Density	mol/cc		0.001071			0.000992	0.001002		0.001099	0.000965		
Mass Density	gm/cc		0.002331			0.002179	0.002201		0.018724	0.003669		
Enthalpy Flow	cal/sec		-0.63727			-0.40941	-0.42364		-8.80103	-1.20E-05		

Average MW			2.17676			2.19533	2.19618	17.0306	3.80206	
Mole Flows	kmol/hr		0.008641			0.008651	0.008651	0.002877	3.36E-08	
WATER	kmol/hr		2.01E-06			1.02E-05	7.39E-06	2.00E-10	4.36E-11	
AMMON-01	kmol/hr		9.04E-05			9.25E-05	9.60E-05	0.002877	3.95E-09	
HYDRO-01	kmol/hr		0.008549			0.008549	0.008548	0	2.96E-08	
Mole Fractions										
WATER			0.000233			0.001177	0.000854	6.96E-08	0.001296	
AMMON-01			0.010467			0.010698	0.011099	1	0.117581	
HYDRO-01			0.989301			0.988126	0.988047	0	0.881123	
Mass Flows	kg/hr		0.01881			0.018993	0.019	0.049	1.28E-07	
WATER	kg/hr		3.62E-05			0.000183	0.000133	3.61E-09	7.85E-10	
AMMON-01	kg/hr		0.00154			0.001576	0.001635	0.049	6.73E-08	
HYDRO-01	kg/hr		0.017233			0.017233	0.017232	0	5.97E-08	
Mass Fractions										
WATER			0.001924			0.009656	0.007003	7.36E-08	0.006141	
AMMON-01			0.081891			0.082988	0.086068	1	0.526681	
HYDRO-01			0.916185			0.907356	0.90693	0	0.467178	
Liquid Phase										
Molar Enthalpy	cal/mol	-16399.5	-58913.5	-49959	-49972	-62626.9	-21683.3	-48521.8	-61259.4	
Mass Enthalpy	cal/gm	-962.946	-3306.62	-2829.27	-2830.1	-3499.26	-1264.62	-2747.87	-3424.82	
Molar Entropy	cal/mol-K	-46.3223	-42.2634	-40.9886	-40.9838	-40.3339	-41.8543	-36.8402	-37.7974	
Mass Entropy	cal/gm-K	-2.71995	-2.37211	-2.32126	-2.32106	-2.25365	-2.44104	-2.08633	-2.11313	
Molar Density	mol/cc	0.033104	0.0452	0.042035	0.042039	0.045531	0.031595	0.038855	0.0439077	
Mass Density	gm/cc	0.563778	0.805325	0.742244	0.74229	0.814883	0.541722	0.6861	0.785374	
Enthalpy Flow	cal/sec	-13.1068	-0.17496	-149.322	-149.366	-0.00725	-14.7539	-145.027	-134.139	

Average MW		17.0306	17.8168	17.6579	17.6574	17.8972	17.1461	17.6579	17.8869
Mole Flows	kmol/hr	0.002877	1.07E-05	0.01076	0.01076	4.16E-07	0.00245	0.01076	0.00788285
WATER	kmol/hr	2.00E-10	8.54E-06	0.006855	0.006858	3.67E-07	0.000287	0.006855	0.00685532
AMMON-01	kmol/hr	0.002877	2.15E-06	0.003905	0.003901	4.99E-08	0.002162	0.003905	0.00102754
HYDRO-01	kmol/hr	0	8.02E-11	0	6.03E-07	4.82E-12	0	0	0
Mole Fractions									
WATER		6.96E-08	0.798563	0.637107	0.637383	0.880223	0.117345	0.637107	0.869649
AMMON-01		1	0.201429	0.362893	0.362561	0.119765	0.882655	0.362893	0.130351
HYDRO-01		0	7.50E-06	0	5.61E-05	1.16E-05	0	0	0
Mass Flows	kg/hr	0.049	0.00019	0.19	0.19	7.45E-06	0.042	0.19	0.141
WATER	kg/hr	3.61E-09	0.000154	0.1235	0.123557	6.60E-06	0.005178	0.1235	0.1235
AMMON-01	kg/hr	0.049	3.67E-05	0.0665	0.066441	8.50E-07	0.036822	0.0665	0.0174996
HYDRO-01	kg/hr	0	1.62E-10	0	1.22E-06	9.71E-12	0	0	0
Mass Fractions									
WATER		7.36E-08	0.807459	0.65	0.650303	0.886032	0.123294	0.65	0.87589
AMMON-01		1	0.19254	0.35	0.349691	0.113966	0.876706	0.35	0.12411
HYDRO-01		0	8.49E-07	0	6.40E-06	1.30E-06	0	0	0

APPENDIX B: EES code for parametric study

```
$UnitSystem SI C kPa kJ mass
$TabStops 0.2  3.5 in

"INPUT PARAMETERS"
P = 2500 [Kpa]                                  "at SHX"
m15 = 0.19 [kg/hr]
Tcond = 35 [C]
Tabs = 38.4 [C]


"GENERATOR, BUBBLE PUMP, SEPARATOR "
m2 = m3 + m4                                    "General mass balance"
m1 = m2
m1 = m15

m2*x2 = m3*x3 + m4*y4                           "x = mass fraction of
ammonia in liquid phase &"
                                                "y = mass fraction of
ammonia in vapor phase"
Qgen = m3*h3 + m4*h4 - m2*h2                    "energy balance at the
generator"

x1 = 0.35
x2 = x1

Q3 = 0
Q4 = 1


 T2 = 128.3 [C]
 h2=enthalpy(NH3H2O,T=T2, P=P, x = x2)
 T4 = T2 - 6
 x15 =x1 - 0.226
 h3=enthalpy(NH3H2O, X=x3, P=P, Q=Q3)
 T3=temperature(NH3H2O, X=x3, P=P, Q=Q3)
 h4=enthalpy(NH3H2O,T=T4, P=P, Q=Q4)
 y4=massfraction(NH3H2O,T=T4, P=P, Q=Q4)


"RECTIFIER"
m4 = m5 + m6                                    "general mass balance"
m4*y4 = m6*y6 + m5*x5                           "ammonia mass
balance"

Qrec = m5*h5 + m6*h6 - m4*h4                    "energy balance at the
rectifier"

y6 = 0.999

Q5 = 0
```

```
Q6 = 1


h6=enthalpy(NH3H2O,x=y6, P=P, Q=Q6)
T6 =temperature(NH3H2O, x=y6, P=P, Q=Q6)
T5 = T6+2
h5=enthalpy(NH3H2O,T=T5, P=P, Q=Q5)
x5= massfraction(NH3H2O, T=T5, P=P, Q=Q5)


"SOLUTION HEAT EXCHANGER"
m15 = m16                                          "mass balance for lean
solution"
x15 = x16
m15 = m3 + m5
m15*x15 = m3*x3 + m5*x5


(m1*h1 + m16*h16) - (m15*h15 + m14*h14) = 0        "energy balance at SHX"

x14 = x1                                           "rich ammonia mass
balance"
Q15 = 0

h1 = h2
h15=enthalpy(NH3H2O,X=x15, P=P, Q=Q15)
T15=temperature(NH3H2O, X=x15, P=P, Q=Q15)
h14=enthalpy(NH3H2O,T=Tabs, P=P, x = x14)


"CONDENSER"
m7 = m6                                            "mass balance"
y7 = y6                                            "ammonia mass
balance"

Qcond = m7*h7 - m6*h6                              "heat balance in the
condenser"
h7=enthalpy(NH3H2O, T=Tcond, P=P, x=y7)


"STATE POINT 10"
T10 = 27.5 [C]
m10tot = 0.019 [Kg/hr]                             "total mass flow of both
ammonia and hydrogen"
y10NH3 = 0.083                                     "mass fraction of
ammonia at point 10"
y10H2 = 0.917

mH2 = y10H2 * m10tot                               "hydrogen mass flow at
point 10"
m10 = y10NH3 * m10tot                              "ammonia mass flow at
point 10"
y10 = 1
y13 = y10
```

"Partial Pressure Calculation at State 10"

P10NH3/P = y10NH3/(y10NH3+molarmass(Ammonia)/molarmass(Hydrogen)*(1-y10NH3))
P10H2 = P - P10NH3

h10 = enthalpy(Ammonia, T=T10, P=P10NH3)

"State POINT 11"
m11 = m10
T11 = T10 - 22
Q11NH3 =1 "Ammonia reaches saturated vapor at 11 from superheated"
h11 = enthalpy(Ammonia, T=T11, x = Q11NH3)

"ABSORBER AND RESERVOIR"

m13 + m16 = m14 + m10 + err_mass "general mass balance"

m13*y13 + m16*x16 = m14*x14 + m10*y10 + err_ammoniaTot "ammonia mass balance"

Qabs = (m14*h14 + m10*h10) - (m13*h13 + m16*h16) "heat rejected in the absorber"
h10H2 = enthalpy(Hydrogen,T=T10,P=P10H2)
h10 = enthalpy(Ammonia, T=T10, P=P10NH3)

{"EXPANSION CHAMBER, EVAPORATOR AND GHX"
Q12 =
m12 = (m7*Q7 + mar)*Q12 "Ammonia after expansion"

{m12L + m12G = m9 + mv} "General mass balance of ammonia after expansion"

{m9 + m11 = m12}
m7 + m10 = m13v
m7*Q7 + mar + m10i = m12v + m12f
m7*Q7 + mar + m10i = m13v + m13f
{m12v + m12f = m13v + m13f}
{m13v =m12}
m9 = m7
m11 = m10

m7*x7 + m10*y10 = m13v*y13 "ammonia mass balance"
y10 = y11
x7 = x9

```
Qevap = (m13v*h13v + m13f*h13f) + mi*Cpi*(T13-T12) - (m12v*h12v + m12f*h12f) +
m7*Q7*(h9-h7) + mi*Cpi*(T11-T10) + mar*(h11-h10) }

"Partial Pressure Calculation at State 12 after expansion"

{y12NH3 = (m11+m9) / (m10tot + m9)
y12H2 = 1 - y12NH3
P12NH3/P = y12NH3/(y12NH3+molarmass(Ammonia)/molarmass(Hydrogen)*(1-
y12NH3))
P12H2 = P - P12NH3}

Q12 = 0.425                                          "Assume vapor fraction
of 80% after expansion"
Q12 = (mH2 + m12v)/(m10tot+m9)
Q12NH3 = m12v/(m11 + m9)                             "Quality of ammonia
after expansion at 12"
y12NH3 = m12v/(mH2 + m12v)
m12 = m9 + m10

P12NH3/P = y12NH3/(y12NH3+molarmass(Ammonia)/molarmass(Hydrogen)*(1-
y12NH3))   "Calculates partial pressure of ammonia after expansion"
P12H2 = P - P12NH3

T12 = t_sat(Ammonia, P=P12NH3)
h12 = enthalpy(Ammonia, P = P12NH3, x = Q12NH3)

"AT STATE POINT 9"
m9 = m7
T9 = Tcond - 30
h9 = enthalpy(Ammonia, T=T9, P=P)

"AT STATE EVAP EXIT"
Te = -5.6 [C]
Qe = 0.643                                           "Assume vapor fraction
of 80% after expansion"
Qe = (mH2 + mev)/(m10tot+m9)
QeNH3 = mev/(m11 + m9)                               "Quality of ammonia
after expansion at 12"
yeNH3 = mev/(mH2 + mev)
me = m12

PeNH3/P = yeNH3/(yeNH3+molarmass(Ammonia)/molarmass(Hydrogen)*(1-
yeNH3))   "Calculates partial pressure of ammonia after expansion"
PeH2 = P - PeNH3

he = enthalpy(Ammonia, T = Te, x = QeNH3)



"At state point 13"

Q13NH3 = 1
m13 = me                                              "The ammonia vapor
leaves the GHX at saturated vapor"
y13NH3 = m13/(mH2+m13)
```

```
P13NH3/P = y13NH3/(y13NH3+molarmass(Ammonia)/molarmass(Hydrogen)*(1-
y13NH3))
P13H2 = P - P13NH3
T13 = 25.3 [C]    {t_sat(Ammonia, P=P13NH3)}
h13 = enthalpy(Ammonia, P=P13NH3, T = T13)


CpH1 = cp(Hydrogen,T=T13 , P= PeNH3)
CpH2 = cp(Hydrogen,T=T12, P= P12NH3)
Qevap = (m13*h13) + mH2*CpH1*(T13-T12) - (m12*h12) + m7*(h9-h7) +
mH2*CpH2*(T11-T10) + m11*(h11-h10)


"OVERALL"
COP = Qevap/Qgen                                    "Coefficient of
Performance of the DAR machine "
MassFlowRatio = m14/m6                              "Mass flow ratio"
```

APPENDIX C: MeteoNorm weather data for Addis Ababa

City	Addis Ababa			
Country	Ethiopia			
Region	Africa			
Source	MeteoNorm 7.1 station			
Latitude	9.03°			
Longitude	38.75°			
Altitude	2448 m			
Time Zone	3 GMT			
Albedo	0.2			
	GlobH	DiffH	Temp	Wind Vel
Month	kWh/m²	kWh/m²	°C	m/s
January	172.7	58.9	16.1	1.6
February	155.9	67.5	17.2	1.49
March	178	77.8	17.8	2
April	160.6	72.2	17.5	2.8
May	159.3	78	18.4	3.19
June	140.5	78.2	17	3.41
July	118.3	71.7	15.5	3.9
August	117.9	69.4	16	4.3
September	137.3	81.3	15.9	4.6
October	172.5	71.7	16.7	4.8
November	182.5	53.5	15.4	3.5
December	176.2	56.4	15.6	1.89
Year	1871.7	836.6	16.6	3.12